JPL Publication 87-39

MSAT-X Report No. 147

The Design of Trellis Codes for Fading Channels

Dariush Divsalar
Marvin K. Simon

November 1, 1987

National Aeronautics and
Space Administration

Jet Propulsion Laboratory
California Institute of Technology
Pasadena, California

The research described in this publication was carried out by the Jet Propulsion Laboratory, California Institute of Technology, under a contract with the National Aeronautics and Space Administration.

TECHNICAL REPORT STANDARD TITLE PAGE

1. Report No. 87-39	2. Government Accession No.	3. Recipient's Catalog No.
4. Title and Subtitle The Design of Trellis Codes for Fading Channels		5. Report Date November 1, 1987 6. Performing Organization Code
7. Author(s) Dariush Divsalar and Marvin K. Simon		8. Performing Organization Report No.
9. Performing Organization Name and Address JET PROPULSION LABORATORY California Institute of Technology 4800 Oak Grove Drive Pasadena, California 91109		10. Work Unit No. 11. Contract or Grant No. NAS7-918 13. Type of Report and Period Covered External Report JPL Publication
12. Sponsoring Agency Name and Address NATIONAL AERONAUTICS AND SPACE ADMINISTRATION Washington, D.C. 20546		14. Sponsoring Agency Code RE4 BP-650-60-15-01-00

15. Supplementary Notes

16. Abstract

It has been well established in the literature that the appropriate criterion for optimum trellis coded modulation design on the additive white Gaussian noise channel is maximization of the free Euclidean distance. We show here that when trellis coded modulation is used on a Rician fading channel with interleaving/deinterleaving, the design of the code for optimum performance is guided by other factors, in particular the length of the shortest error event path, and the product of branch distances (possibly normalized by the Euclidean distance of the path) along that path. Although maximum free distance (d_{free}) is still an important consideration, it plays a less significant role the more severe the fading is on the channel. These considerations lead to the definition of a new distance measure for optimization of trellis codes transmitted over Rician fading channels. If no interleaving/deinterleaving is used, then once again the design of the trellis code is guided by maximizing d_{free}.

It is also shown that allowing for multiple symbols per trellis branch, i.e., multiple trellis coded modulation (MTCM), provides an additional degree of freedom for designing a code to meet the above optimization criteria on the fading channel. It is here where the MTCM technique exploits its full potential.

17. Key Words (Selected by Author(s))	18. Distribution Statement
Communications	Unclassified; unlimited

19. Security Classif. (of this report)	20. Security Classif. (of this page)	21. No. of Pages	22. Price
Unclassified	Unclassified		

Abstract

It has been well established in the literature that the appropriate criterion for optimum trellis coded modulation design on the additive white Gaussian noise channel is maximization of the free Euclidean distance. We show here that when trellis coded modulation is used on a Rician fading channel with interleaving/deinterleaving, the design of the code for optimum performance is guided by other factors, in particular the length of the shortest error event path, and the product of branch distances (possibly normalized by the Euclidean distance of the path) along that path. Although maximum free distance (d_{free}) is still an important consideration, it plays a less significant role the more severe the fading is on the channel. These considerations lead to the definition of a new distance measure for optimization of trellis codes transmitted over Rician fading channels. If no interleaving/deinterleaving is used, then once again the design of the trellis code is guided by maximizing d_{free}.

It is also shown that allowing for multiple symbols per trellis branch, i.e., multiple trellis coded modulation (MTCM), provides an additional degree of freedom for designing a code to meet the above optimization criteria on the fading channel. It is here where the MTCM technique exploits its full potential.

CONTENTS

Introduction

In previous publications [1-4], the authors have considered the performance of conventional and multiple trellis codes in a Rician fading environment characteristic of the mobile satellite channel. Results were reported for both the case of coherent detection and differentially coherent detection with and without the use of channel state information (CSI). The primary emphasis in these previous works was the degradation in performance produced by the fading for trellis codes designed to be optimum on the additive Gaussian noise channel (AWGN).

In this report, we look more carefully into the properties of the trellis coded modulation (TCM) that enter into the various expressions for average bit error probability corresponding to the above-mentioned cases and then proceed to use these as design criteria for conventional and multiple trellis codes operating over a fading channel. It is shown that, whereas maximizing free Euclidean distance (d_{free}) is the appropriate optimum design criterion on the AWGN, over Rician fading channels with interleaving/deinterleaving, the asymptotic performance of TCM at high signal-to-noise ratio (SNR) is dominated by several other factors depending on the value of the Rician parameter K, i.e., the ratio of direct plus specular power (coherent components) to diffuse power (noncoherent component). In particular, for small values of K (the channel tends toward Rayleigh), the primary design criteria for high SNR become: 1) the <u>length</u> (to be defined in the report) of the shortest error event path, and 2) the <u>product</u> of branch distances along that path, with d_{free} a secondary consideration. Thus, at low values of K, the longer is the shortest error event path and the larger is the product of the branch distances along that path, the better the code will perform <u>even though d_{free} does not achieve its optimum value over the AWGN</u>! As K increases, the significance of these primary and secondary considerations shift relative to one another until K reaches infinity (AWGN), in which case optimum performance is once again achieved by a trellis code designed to maximize d_{free}.

To demonstrate the above analytically, our approach will be to first take the previously derived [1-4] upper bounds on average error probability performance in the presence of fading and investigate their asymptotic behavior as SNR

gets large. A comparison of these results for the different cases, i.e., coherent versus differentially coherent detection and CSI versus no CSI, will reveal some striking similarities with regard to the way in which certain properties of the trellis code design affect the rate of descent of average error probability with average SNR. When these properties are used as a motivation for good code design, we then show that multiple trellis coded modulation (MTCM) [4], wherein more than one channel symbol is assigned to each trellis branch, is a natural choice in this situation. In fact, we will show that MTCM allows us to achieve a performance on the fading channel superior to that achievable by a conventional (single channel symbol per trellis branch) TCM of the same throughput and number of trellis states.

Since conventional TCM can be viewed as a special case of multiple TCM [4], we shall begin our detailed discussion with a description of the system model for the more general MTCM.

System Model

The system under consideration is illustrated by the block diagram in Figure 1. The elements indicated in dashed lines represent system functions that are peculiar to the form of detection, i.e., coherent versus differentially coherent. In particular, the differential encoder is required for differentially coherent detection but not coherent detection. Similarly, the injection of a pilot tone at the transmitter and its extraction at the receiver for purposes of demodulation are required for coherent detection but not differentially coherent detection. All other blocks have similar system functions for both forms of detection.

The key elements of Figure 1, as far as our interest in this report is concerned, are the trellis encoder and the MPSK signal set mapping.* A multiple trellis encoder has b binary input bits and s binary output symbols which are mapped into k M-ary symbols in each transmission interval (see

*In keeping with our previous work [1-4] on the performance of TCM over fading channels, we consider only MPSK modulation.

Figure 2). For such a transmitter, the throughput is b/k bps/Hz which has a unity bandwidth expansion relative to an uncoded system with a $2^{b/k}$-point signal constellation.

One way of producing such a result is to partition the s binary encoder output symbols into k groups of $m = \log_2 M$ symbols each. Each of these groups results in an MPSK output symbol. Clearly, to achieve this result, the transmitter parameters s, k, and M must be chosen such that $s = k \log_2 M$.

Another possibility is to partition the s binary encoder output into k groups of symbols where each group now corresponds to, in general, a different size MPSK signal set. Thus, if, for the ith group, $m_i = \log_2 M_i$, then we require $s = m_1 + m_2 + \ldots, + m_k$. Another interpretation of this requirement is in terms of the total number of multiple signals 2^{b+1} used in the trellis diagram. Since, for any encoder, $s \geq b+1$, then $m_1, m_2, \ldots, m_k$ must be chosen such that $2^{\sum m_i}$ is greater than the total number of multiple signals required in the trellis diagram. If M is not a power of 2 then the equivalent requirement is $2^{b+1} \leq \prod_{i=1}^{k} M_i$.

In keeping with our previous work on MTCM, we shall emphasize the former partition, i.e., k equal size groups, but also allow for the latter partition in terms of an example. A complete exposition of the applications and advantages of partitioning into unequal group sizes is the subject of a future paper by the authors.

Asymptotic Performance Analysis

A. Ideal Interleaving/Deinterleaving

An upper bound on the average bit error probability is obtained as

$$P_b \leq \sum_{\underline{x},\hat{\underline{x}}} \sum_{\mathscr{C}} a(\underline{x},\hat{\underline{x}}) p(\underline{x}) P(\underline{x} \rightarrow \hat{\underline{x}}) \qquad (1)$$

where $a(\underline{x},\hat{\underline{x}})$ is the number of bit errors that occur when the sequence $\underline{x}$ is transmitted and the sequence $\hat{\underline{x}} \neq \underline{x}$ is chosen by the decoder, $p(\underline{x})$ is the a

priori probability of transmitting $\underline{x}$, and $\mathscr{C}$ is the set of all coded sequences. Also, in (1), $P(\underline{x} \rightarrow \hat{\underline{x}})$ represents the pairwise error probability, i.e., the probability that the decoder chooses $\hat{\underline{x}}$ when indeed $\underline{x}$ was transmitted. The upper bound of (1) is efficiently evaluated using the transfer function bound approach applied to TCM in [1-5].

Evaluation of the pairwise error probability depends on the proposed decoding metric, the presence or absence of CSI, and the type of detection used, i.e., coherent versus differentially coherent. For example, consider the case of coherent detection with ideal (perfect) CSI and a Gaussian decoding metric (correlation metric). For this case, it has been shown ([1], Equations (20) - (21)) that, conditioned on the fading amplitude vector $\underline{\rho} = (\rho_1, \rho_2, \ldots \rho_n)$, the pairwise error probability is given by

$$P(\underline{x} \rightarrow \hat{\underline{x}}|\underline{\rho}) \leq \exp\left\{-\frac{E_s}{4N_0} d^2(\underline{x},\hat{\underline{x}})\right\} \tag{2a}$$

where

$$d^2(\underline{x},\hat{\underline{x}}) \triangleq \sum_{n\in\eta} \rho_n^2 |x_n - \hat{x}_n|^2 \tag{2b}$$

represents the square of the weighted Euclidean distance between the two symbol sequences $\underline{x}$ and $\hat{\underline{x}}$ and η is the set of all n for which $x_n \neq \hat{x}_n$. In (2b), ρ_n is the normalized fading amplitude for the nth transmission interval which for Rician fading has the probability density function (independent of n)

$$p(\rho) = \begin{cases} 2\rho(1 + K) \exp\left[-K - \rho^2(1 + K)I_0(2\rho\sqrt{K(1 + K)}\right); \ \rho \geq 0 \\ 0 \ ; \text{ otherwise} \end{cases} \tag{3}$$

where $I_0(x)$ is the zero-order modified Bessel function of the first kind. Also, in (2a), E_s/N_0 is the M-ary channel symbol energy to noise spectral density ratio. For multiple trellis coding, the symbol energy E_s is related to the bit energy E_b by $E_s = (b/k)E_b$.

For ideal interleaving/deinterleaving, the ρ_n's in (2b) are independent and, as noted above, identically distributed. Thus, averaging (2a) over the probability density function of (3) gives [1]

$$P(\underline{x} \to \hat{\underline{x}}) \le \prod_{n \in \eta} \frac{1 + K}{1 + K + \frac{\bar{E}_s}{4N_0} |x_n - \hat{x}_n|^2} \exp\left\{ - \frac{K \frac{\bar{E}_s}{4N_0} |x_n - \hat{x}_n|^2}{1 + K + \frac{\bar{E}_s}{4N_0} |x_n - \hat{x}_n|^2} \right\} \quad (4)$$

which can be written in the form

$$P(\underline{x} \to \hat{\underline{x}}) \le \exp\left(- \frac{\bar{E}_s}{4N_0} d^2 \right) \quad (5a)$$

with*

$$d^2 = \sum_{n \in \eta} \left\{ \underbrace{\frac{|x_n - \hat{x}_n|^2 K}{1 + K + \frac{\bar{E}_s}{4N_0} |x_n - \hat{x}_n|^2}}_{d_{1n}^2} + \underbrace{\left(\frac{\bar{E}_s}{4N_0} \right)^{-1} \ln\left(\frac{1 + K + \frac{\bar{E}_s}{4N_0} |x_n - \hat{x}_n|^2}{1 + K} \right)}_{d_{2n}^2} \right\} \quad (5b)$$

Note that for $K = \infty$ (no fading),

$$\begin{aligned} d_{1n}^2 &= |x_n - \hat{x}_n|^2 \\ d_{2n}^2 &= 0 \end{aligned} \quad (6a)$$

and thus d^2 is merely the sum of the squared Euclidean distances along the error event path.

---

*Note that d satisfies the conditions for a distance metric (see Appendix A).

For K = 0 (Rayleigh fading),

$$d_{1n}^2 = 0$$

$$d_{2n}^2 = \left(\frac{\bar{E}_s}{4N_0}\right)^{-1} \ln\left(1 + \frac{\bar{E}_s}{4N_0} |x_n - \hat{x}_n|^2\right) \tag{6b}$$

and thus for reasonably large $\bar{E}_s/N_0$ values, d^2 is the sum of the logarithms of the squared Euclidean distances (each weighted by $\bar{E}_s/4N_0$).

Equivalently, the upper bound on pairwise error probability for this special case becomes

$$P(\underline{x} \to \hat{\underline{x}}) \leq \left(\prod_{n \in \eta} \frac{\bar{E}_s}{4N_0} |x_n - \hat{x}_n|^2\right)^{-1} \tag{7}$$

i.e., it is proportional to the product of the squared Euclidean distances along the error event path.

For values of K between 0 and ∞, the equivalent squared Euclidean distance, d^2, will be a mixture of the above two special cases. We now turn our attention to asymptotic behavior.

At sufficiently high SNR, (4) simplifies to

$$P(\underline{x} \to \hat{\underline{x}}) \leq \prod_{n \in \eta} \frac{1}{\left(\frac{\bar{E}_s}{N_0}\right)^{\frac{|x_n - \hat{x}_n|^2}{4(1+K)}}} e^{-K} \tag{8}$$

Substituting (8) into (1), we get

$$P_b \leq \sum_{\underline{x}, \hat{\underline{x}}} \sum_{\varepsilon \mathscr{E}} a(\underline{x}, \hat{\underline{x}})\, p(\underline{x}) \prod_{n \in \eta} \frac{1}{\left(\frac{\bar{E}_s}{N_0}\right)^{\frac{|x_n - \hat{x}_n|^2}{4(1+K)}}} e^{-K} \tag{9}$$

whose evaluation depends on the particular trellis code design.

To identify the important considerations for such a design in a fading environment, we first observe that the upper bound of (9) will be dominated by the term in the summation which has the slowest rate of descent with $\bar{E}_s/N_0$. This in turn corresponds to the error event path with the smallest number of elements in η. We refer to this path as the "shortest error event path" and define it more formally as the error event path with the smallest number of nonzero distances between itself and the correct path. We also define the "length", L, of the shortest error event path by the number of nonzero pairwise distances between the symbols along its branches and those along the correct path. It is to be emphasized that pairwise distance refers to Euclidean distance between corresponding symbols on the pair of paths being compared.

In terms of the above definitions, we see that asymptotically with high SNR, the average bit error probability is approximately given by*

$$P_b \cong \frac{1}{b} C \left(\frac{(1+K)e^{-K}}{\bar{E}_s/N_0} \right)^L ; \quad \bar{E}_s/N_0 >> K \tag{10}$$

where C is a constant that depends on the distance structure of the code. For now, the important point to be observed in (10) is that P_b varies inversely with $(\bar{E}_s/N_0)^L$.

For conventional trellis coding, wherein each branch in the trellis corresponds to a single MPSK output channel symbol, the shortest error event path is that error event path with the fewest number of branches having nonzero pairwise distance from the correct path. For most cases, this also corresponds to the shortest length (in branches) error event and thus L is just the number of branches on this path.

---

*The approximation in (10) stems from the fact that we consider only a single term in (9), namely, that due to the shortest (in length) error event path. Also, for simplicity, we shall ignore the number of such paths in the computation of C. As such, (10) also represents a strict lower bound on P_b.

For multiple trellis coding, wherein each branch in the trellis corresponds to more than one MPSK output channel symbol, the "length" of the shortest error event path is always equal to or greater than the number of branches along the shortest error event path. In view of (10), the possibility of a value of L greater than the length (in branches) of the shortest error event path is significant and what affords multiple trellis coding the opportunity of improving trellis coding performance on the fading channel. A simple example of this comment, which will be explored in a more general context later on in the report, pertains to trellis diagrams with parallel paths between states. This occurs whenever 2^b, i.e., the number of possible transitions from a given state, exceeds the number of states of the trellis diagram. In such cases, with conventional trellis coding, the minimum distance error event path is often the parallel path, i.e., the shortest error event path is of length one branch, and thus L = 1. With MTCM, we have the option of still having a trellis diagram with parallel paths, yet because of the multiplicity, we can have more than one nonzero pairwise Euclidean distance along that path; hence the opportunity of achieving a value of L greater than one.

As a second example, consider the case of differentially coherent detection of MPSK (i.e., MDPSK) with no CSI and a Gaussian decoding metric. Although this metric is suboptimum for MDPSK, it was shown in [4] that it is considerably easier to implement than the true optimum metric and thus of significant practical interest. From Equations (25) and (26) of [4], the upper bound on pairwise error probability for the Rician channel is given by

$$P(\underline{x} \to \hat{\underline{x}}) \le \prod_{n \in \eta} \frac{1 + K}{1 + K + |x_n - \hat{x}_n|^2 \left[2\lambda \frac{\bar{E}_s}{N_0} (1-4\lambda) - (2\lambda)^2 (1+K) \right]}$$

$$\times \exp\left\{ - \frac{2\lambda K \frac{\bar{E}_s}{N_0} (1-4\lambda) |x_n - \hat{x}_n|^2}{1 + K + |x_n - \hat{x}_n|^2 \left[2\lambda \frac{\bar{E}_s}{N_0} (1-4\lambda) - (2\lambda)^2 (1+K) \right]} \right\} \quad (11)$$

where λ is a Chernoff bound parameter to be optimized. For the Rayleigh channel (K=0), (11) simplifies to

$$P(\underline{x} \to \hat{\underline{x}}) \leq \prod_{n \in \eta} \frac{1}{1 + |x_n - \hat{x}_n|^2 \left[2\lambda \frac{\bar{E}_s}{N_0} (1-4\lambda) - (2\lambda)^2 \right]} \tag{12}$$

The bound in (11) cannot be optimized over λ independent of the index n. On the other hand, the result in (12) can be optimized over λ independent of n. In particular, differentiating the expression in brackets in (12) with respect to λ and equating the result to zero gives the optimum Chernoff parameter for the Rayleigh channel, namely,

$$\lambda_{opt} = \frac{\frac{\bar{E}_s}{4N_0}}{1 + 2\frac{\bar{E}_s}{N_0}} \tag{13}$$

For high SNR, (13) simplifies to

$$\lambda_{opt} \cong \frac{1}{8} \tag{14}$$

Although (14) is not the optimum value of λ for (11), we use it nevertheless (resulting in a looser upper bound) to arrive at a result in a desirable form. Thus, substituting (13) in (11) gives

$$P(\underline{x} \to \hat{\underline{x}}) \leq \prod_{n \in \eta} \frac{1 + K}{1 + K + \frac{|x_n - \hat{x}_n|^2}{16} \left[2\frac{\bar{E}_s}{N_0} - (1+K) \right]}$$

$$\times \exp\left\{ - \frac{K\left(\frac{\bar{E}_s}{8N_0}\right)|x_n - \hat{x}_n|^2}{1 + K + \frac{|x_n - \hat{x}_n|^2}{16} \left[2\frac{\bar{E}_s}{N_0} - (1+K) \right]} \right\}$$

$$= \exp\left(-\frac{\bar{E}_s}{4N_0} d^2\right) \tag{15a}$$

where, analogous to (5b),

$$d^2 = \sum_{n\epsilon\eta} \left\{ \frac{\frac{1}{2}|x_n - \hat{x}_n|^2 K}{1 + K + \frac{|x_n - \hat{x}_n|^2}{16}\left[2\frac{\bar{E}_s}{N_0} - (1+K)\right]} + \left(\frac{\bar{E}_s}{4N_0}\right)^{-1} \ln\left(\frac{1 + K + \frac{|x_n - \hat{x}_n|^2}{16}\left[2\frac{\bar{E}_s}{N_0} - (1+K)\right]}{1 + K}\right)\right\} \tag{15b}$$

is a distance metric for $\bar{E}_s/N_0 > (1+K)/2$.

For sufficiently high SNR, (15) can be further approximated by

$$P(\underline{x} \to \hat{\underline{x}}) \lesssim \prod_{n\epsilon\eta} \frac{1}{\left(\frac{\bar{E}_s}{N_0}\right)\frac{|x_n - \hat{x}_n|^2}{8(1+K)}} e^{-K} \tag{16}$$

Finally, using (16) in (1), we get

$$P_b \leq \sum_{\underline{x},\hat{\underline{x}}} \sum_{\epsilon \mathscr{E}} a(\underline{x},\hat{\underline{x}}) p(\underline{x}) \prod_{n\epsilon\eta} \frac{1}{\left(\frac{\bar{E}_s}{N_0}\right)\frac{|x_n - \hat{x}_n|^2}{8(1+K)}} e^{-K} \tag{17}$$

which is identical to (9) except for a scale factor and thus can be written in the form of (10).

As a third example, consider once again the case of coherent detection of MPSK, now, however, with no CSI. From Equations (28) and (29b) of [1], the upper bound on pairwise error probability for the Rician channel is given by

$$P(\underline{x} \to \hat{\underline{x}}) \le \prod_{n\epsilon\eta} \overline{\exp\left\{-\frac{\bar{E}_s}{N_0}\lambda(\rho_n - \lambda)|x_n - \hat{x}_n|^2\right\}}^{\rho_n}$$

$$= \prod_{n\epsilon\eta} \exp\left(\lambda^2 \frac{\bar{E}_s}{N_0}|x_n - \hat{x}_n|^2\right)\overline{\exp\left(-\frac{\bar{E}_s}{N_0}\lambda\rho_n|x_n - \hat{x}_n|^2\right)}^{\rho_n} \qquad (18)$$

The expectation over the Rician probability density function of (3) is performed in [1], which reduces (18) to

$$P(\underline{x} \to \hat{\underline{x}}) \le \prod_{n\epsilon\eta} \exp\left(\lambda^2 \frac{\bar{E}_s}{N_0}|x_n - \hat{x}_n|^2\right)$$

$$x\ e^{-K}\left[1 - \frac{1}{\sqrt{\pi}}\int_0^{\pi} \eta(\theta)\exp(\eta^2(\theta))\operatorname{erfc}\eta(\theta)\,d\theta\right] \qquad (19)$$

where

$$\eta(\theta) = \frac{\lambda|x_n - \hat{x}_n|^2 \frac{\bar{E}_s}{2N_0}}{\sqrt{1+K}} - \sqrt{K}\cos\theta \qquad (20)$$

For sufficiently large $\bar{E}_s/N_0$, the first term of (20) dominates, in which case $\eta(\theta)$ becomes independent of θ and the evaluation of the integral becomes trivial. Thus, approximating (20) by its first term allows (19) to be simplified to

$$P(\underline{x} \to \hat{\underline{x}}) \le \prod_{n\epsilon\eta} \exp\left(\lambda^2 \frac{\bar{E}_s}{N_0}|x_n - \hat{x}_n|^2\right)$$

$$x\ e^{-K}\left[1 - \sqrt{\pi}\,\lambda\,|x_n - \hat{x}_n|^2\left(\frac{\bar{E}_s}{2N_0}\right)\right]$$

$$\times \exp\left\{\left[\left[\lambda|x_n - \hat{x}_n|^2 \frac{\bar{E}_s}{2N_0}\right]^2\right\}\operatorname{erfc}\left(\lambda|x_n - \hat{x}_n|^2 \frac{\bar{E}_s}{2N_0}\right)\right. \tag{21}$$

Furthermore, since for large $\bar{E}_s/N_0$ we can use the asymptotic expansion for the complementary error function, namely,

$$\operatorname{erfc} x \cong \frac{\exp(-x^2)}{\sqrt{\pi}\, x}\left(1 - \frac{1}{2x^2}\right) \tag{22}$$

then, using (22) in (21) gives the further simplification

$$P(\underline{x} \to \hat{\underline{x}}) \le \prod_{n\epsilon\eta} \frac{\exp\left(\lambda^2 \frac{\bar{E}_s}{N_0}|x_n - \hat{x}_n|^2\right)}{2\lambda^2|x_n - \hat{x}_n|^4\left(\frac{\bar{E}_s}{2N_0}\right)^2}$$

$$= \frac{\exp\left(\lambda^2 \frac{\bar{E}_s}{N_0}\sum_{n\epsilon\eta}|x_n - \hat{x}_n|^2\right)}{2^{L_\eta}\lambda^{2L_\eta}\left(\frac{\bar{E}_s}{2N_0}\right)^{2L_\eta}\prod_{n\epsilon\eta}|x_n - \hat{x}_n|^4} \tag{23}$$

where L_η is the "length" of the error event path corresponding to $\hat{\underline{x}}$, i.e., the number of elements in η.

The result in (23) can be optimized over the Chernoff parameter. Performing this optimization gives

$$\lambda^2_{opt} = \frac{L_\eta}{\frac{\bar{E}_s}{N_0}\sum_{n\epsilon\eta}|x_n - \hat{x}_n|^2} \tag{24}$$

which, when substituted in (23), gives the tightest upper bound on pairwise error probability, namely,

$$P(\underline{x} \to \hat{\underline{x}}) \le \frac{e^{L_\eta}}{2^{L_\eta}\left(\frac{\bar{E}_s}{2N_0}\right)^{2L_\eta}\left(\frac{L_\eta}{\frac{\bar{E}_s}{N_0}\sum_{n\epsilon\eta}|x_n - \hat{x}_n|^2}\right)\prod_{n\epsilon\eta}|x_n - \hat{x}_n|^4}$$

$$= \frac{\left(\frac{2e}{L_\eta}\right)^{L_\eta}\left(\sum_{n\epsilon\eta}|x_n - \hat{x}_n|^2\right)^{L_\eta}}{\left(\frac{\bar{E}_s}{N_0}\right)^{L_\eta}\left(\prod_{n\epsilon\eta}|x_n - \hat{x}_n|^2\right)^2} = \frac{\left(\frac{2e}{L_\eta}\right)^{L_\eta}}{\left(\frac{\bar{E}_s}{N_0}\right)^{L_\eta}}\left(\prod_{n\epsilon\eta}\frac{|x_n - \hat{x}_n|^2}{\left(\sum_{n\epsilon\eta}|x_n - \hat{x}_n|^2\right)^{1/2}}\right)^{-2} \qquad (25)$$

Finally, substitution of (25) in (1) allows computation of the upper bound on bit error probability, which once again can be put in the form of (10), where L would be the smallest value of L_η. The primary difference between this third example and the previous two is the manner in which the constant C in (10) depends on the distance structure of the trellis code. More about that later on.

An Example

Consider a rate 1/2 trellis coded 4PSK modulation with the 2-state diagram illustrated in Figure 3. Each branch of this diagram is labeled with the 4PSK symbol transmitted when making that particular transition. The shortest error event path is of length 2 branches and both of these have nonzero distance with respect to the branches of the correct path (assumed to be the all zeros path). Thus, the "length" L of the shortest error event path is equal to two.

For coherent detection without CSI, we need to compute the ratio of the sum of the squared branch distances to the product of the squared branch distances in accordance with (25). From Figure 3, the square of this ratio is easily computed as

$$\left(\frac{\sum_{n\epsilon\eta}|x_n - \hat{x}_n|^2}{\prod_{n\epsilon\eta}|x_n - \hat{x}_n|^2}\right)^2 = \frac{(4+2)^2}{(4x2)^2} = \frac{36}{64} = \frac{9}{16} \qquad (26)$$

Thus, letting $L_\eta = 2$ in (25), $\bar{E}_s = \bar{E}_b$, and substituting (26) into this same equation gives the upper bound on pairwise error probability

$$P(\underline{x} \to \hat{\underline{x}}) \leq \frac{e^2 e^{-2K(1+K)^2}}{\left(\frac{\bar{E}_b}{N_0}\right)^2} \left(\frac{\sum_{n \in \eta} |x_n - \hat{x}_n|^2}{\prod_{n \in \eta} |x_n - \hat{x}_n|^2} \right)^2$$

$$= \frac{9e^2 e^{-2K(1+K)^2}}{16\left(\frac{\bar{E}_b}{N_0}\right)^2} \tag{27}$$

which, for large $\bar{E}_b/N_0$, is also approximately equal to the upper bound on bit error probability. Letting K=0 gives the identical result obtained in [1, Equation (67)] for the Rayleigh case.

For coherent detection with CSI, we need to compute the product of the branch distances in accordance with (9). For the shortest error event path this product is easily computed as

$$\prod_{n \in \eta} |x_n - \hat{x}_n|^2 = 4 \times 2 = 8 \tag{28}$$

Thus, keeping only the term in (9) corresponding to the shortest error event path we get

$$P_b \cong \frac{1}{\left(\frac{\bar{E}_b}{N_0}\right)^2 \frac{\prod_{n \in \eta} |x_n - \hat{x}_n|^2}{[4(1+K)]^2}} e^{-2K}$$

$$= \frac{2e^{-2K(1+K)^2}}{\left(\frac{\bar{E}_b}{N_0}\right)^2} \tag{29}$$

which for K=0 agrees with [1, Equation (49')]*.

Finally, for differentially coherent detection with no CSI, (17) also requires calculation of the product of branch distances. Using (28) and again keeping only the term in (17) corresponding to this path, we get

$$P_b \cong \frac{1}{\left(\frac{\bar{E}_b}{N_0}\right)^2 \frac{\prod_{n\epsilon\eta} |x_n - \hat{x}_n|^2}{[8(1+K)]^2}} e^{-2K}$$

$$= \frac{8e^{-2K}(1+K)^2}{\left(\frac{\bar{E}_b}{N_0}\right)^2} \tag{30}$$

which, for K=0, agrees with (56a) of [4].

B. No Interleaving/Deinterleaving

If no interleaving/deinterleaving is employed, then the assumption that the fading is independent from symbol to symbol is no longer valid. In fact, if the fading is sufficiently slow as to be constant over the duration of a number of symbols equal to the minimum distance error event path, then for coherent detection with a Gaussian metric, the average bit error probability is asymptotically upper bounded by

$$P_b \cong C_1 \overline{\exp\left(-\rho^2 d_{free}^2 \frac{\bar{E}_s}{4N_0}\right)}^{\rho} \tag{31}$$

where C_1 is a constant, d_{free}^2 is the squared free distance of the code, i.e.,

$$d_{free}^2 = \min \sum_{n\epsilon\eta} |x_n - \hat{x}_n|^2 \tag{32}$$

*Equation (49') of [1] should be corrected to read $P_b \cong \frac{1}{(\bar{E}_b/\sqrt{2}N_0)^2}$

and the overbar denotes averaging over the Rician probability density function of (3). Performing this average gives

$$P_b \cong C_1 \frac{1+K}{1+K+C_2} \exp\left(-K \frac{C_2}{1+K+C_2}\right); \quad C_2 = d_{free}^2 \frac{\bar{E}_s}{4N_0} \tag{33}$$

which can be approximated for large $\bar{E}_s/N_0$ by

$$P_b \cong C \frac{1+K}{d_{free}^2 \frac{\bar{E}_s}{N_0}} e^{-K} \tag{34}$$

where

$$C = 4C_1.$$

For differentially coherent detection with a Gaussian metric, the analogous result to (31) is obtained from [4; Equation (25)] and is given by

$$P_b \lesssim \min_{\lambda_0} C_1' \frac{\exp\left\{-2\lambda_0\rho^2 \frac{\bar{E}_s}{N_0} \sum_{n\varepsilon\eta} \frac{|x_n-\hat{x}_n|^2(1-4\lambda_0)}{1-(2\lambda_0)^2|x_n-\hat{x}_n|^2}\right\}}{\prod_{n\varepsilon\eta}\left[1-(2\lambda_0)^2|x_n-\hat{x}_n|^2\right]}^{\rho} \tag{35}$$

where η corresponds to the dominant error event path. Again performing the average over the fading probability density function gives

$$P_b \lesssim \min_{\lambda_0} C_1' \frac{\frac{1+K}{1+K+C_2} \exp\left(-K \frac{C_2}{1+K+C_2}\right)}{\prod_{n\varepsilon\eta}\left[1-(2\lambda_0)^2|x_n-\hat{x}_n|^2\right]};$$

$$C_2 = 2\lambda_0 \frac{\bar{E}_s}{N_0} \sum_{n\varepsilon\eta} \frac{|x_n-\hat{x}_n|^2(1-4\lambda_0)}{1-(2\lambda_0)^2|x_n-\hat{x}_n|^2} \tag{36}$$

which for large $\bar{E}_s/N_0$ simplifies to

$$P_b \lesssim \min_{\lambda_0} \frac{C_1' (1+K) e^{-K}}{C_2 \prod_{n\varepsilon\eta} [1-(2\lambda_0)^2|x_n-\hat{x}_n|^2]}$$

$$= \min_{\lambda_0} \frac{C_1' (1+K) e^{-K}}{2\lambda_0 (1-4\lambda_0) \left(\frac{\bar{E}_s}{N_0}\right) \sum_{n\varepsilon\eta} |x_n-\hat{x}_n|^2 \prod_{\substack{k\varepsilon\eta \\ k\neq n}} [1-(2\lambda_0)^2|x_n-\hat{x}_n|^2]} \qquad (37)$$

which, when optimized over the Chernoff parameter, can be put in the form of (34).

Thus, for either coherent or differentially coherent detection, comparing (34) with (10), we observe that, with no interleaving/deinterleaving, <u>independent of the trellis code</u>, the asymptotic steepest rate of descent of P_b with $\bar{E}_s/N_0$ is inverse linear.

<u>Multiple Trellis Coded Design for Fading Channels</u>

In this section, we expand upon the brief comments previously made about the suitability of using multiple trellis codes on the fading channel. In particular, we shall demonstrate that multiple trellis coding has the ability to produce a performance behavior that otherwise would not be achievable with conventional trellis coded MPSK of the same effective code rate, complexity (number of trellis states), and number of signal points M.

Recall that with conventional trellis coding (i.e., one symbol per trellis branch) the length L of the shortest error event path is equal to the number of trellis branches along that path. Equivalently, if we assume that the all zeros path in the trellis diagram represents the transmitted sequence, then L is the number of branches in the shortest length path to which a non-zero MPSK symbol is associated. Since a trellis diagram with parallel paths is

constrained to have a shortest error event of length one branch, we immediately have L = 1, i.e., the average bit error probability asymptotically varies inverse linearly with $\bar{E}_s/N_0$. Thus, we conclude that for conventional trellis coding on the fading channel, from an error probability performance standpoint, it is undesirable to design the code to have parallel paths in its trellis diagram. Unfortunately, however, for a conventional rate n/(n+1) trellis code, when 2^n exceeds the number of states, one is forced into a trellis with parallel paths. Thus, in these instances, there is no choice but to accept an inverse linear asymptotic performance on the fading channel.

When multiple trellis coding is employed, we regain the option of designing a trellis diagram with parallel paths yet still being able to achieve an asymptotic performance on the fading channel which varies inversely with $\bar{E}_s/N_0$ at a rate faster than linear. The reason behind this lies in the fact that even if there exist parallel paths in the trellis, it is now possible to have more than one MPSK symbol with non-zero Euclidean distance associated with an error event of length one branch. In fact, even if the multiplicity, k, is equal to just two, as long as all of the pairs of MPSK symbols assigned to the parallel paths are not alike in either of the two symbol positions, i.e., they both represent non-zero Euclidean distances, then the pairwise error probability associated with that error event path will vary inversely with the square of $\bar{E}_s/N_0$. Thus, the primary objective for good multiple trellis code design on the fading channel is to maximize the number of symbols with non-zero Euclidean distance along the error event path of shortest length. A secondary objective is to minimize the constant C in (10), which, depending on the detection scheme (i.e., coherent or differentally coherent), requires either maximizing the product of the squared branch distances or maximizing the product of the squared branch distances each normalized by the square root of their sum along this shortest length path.

The simplest way of illustrating the above considerations is with an example. In [5], we consider the design of rate 2/3 conventional trellis coded 8PSK systems for the AWGN. In particular, for the 2-state case, the trellis diagram is illustrated in Figure 4. Since for a rate 2/3 code there are $2^2 = 4$ possible transitions from each state to the next state, a conventional 2-state trellis must have 2 parallel paths between states. In

Figure 4, these parallel paths are labeled with the MPSK output symbol transmitted over the channel when that particular transition occurs.

The performance of this conventional TCM scheme used on the Rician fading channel with coherent detection at the receiver is given in [3]. Because of the existence of parallel paths in Figure 4, this performance will asymptotically (for sufficiently large $\bar{E}_s/N_0$) vary inversely with $\bar{E}_s/N_0$. In particular, since, for the parallel paths, $|x_n - \hat{x}_n|^2 = 4$, then, for example, for coherent detection with ideal CSI, the dominant term of (9) yields

$$P_b \lesssim \frac{1}{2}\frac{1+K}{\left(\frac{\bar{E}_s}{N_0}\right)}e^{-K} = \frac{1}{4}\frac{1+K}{\left(\frac{\bar{E}_b}{N_0}\right)}e^{-K} \tag{38}$$

where we have also noted that for a rate 2/3 code, $\bar{E}_s = 2\bar{E}_b$.

Now consider the rate 4/6 (=2/3), 2 state multiple (k=2) trellis code, with the trellis diagram illustrated in Figure 5. For this code b=4, s=6, and thus there are $2^b = 16$ possible paths leaving each state. Since there are only 2 states, each transition between states has 8 parallel paths. The sets of 8PSK symbol pairs for these transitions are illustrated directly on the branches of the trellis diagram and correspond to the signal points in the 8PSK signal constellation as shown. The construction of these sets is given below.

$$A = \begin{bmatrix} 0 & 0 \\ 4 & 4 \end{bmatrix} \qquad B = A + [2\ 2] = \begin{bmatrix} 2 & 2 \\ 6 & 6 \end{bmatrix}$$

$$C = A\ U\ B = \begin{bmatrix} 0 & 0 \\ 2 & 2 \\ 4 & 4 \\ 6 & 6 \end{bmatrix} \qquad D = C + [1\ 5] = \begin{bmatrix} 1 & 5 \\ 3 & 7 \\ 5 & 1 \\ 7 & 3 \end{bmatrix}$$

$$E = C\ U\ D = \begin{bmatrix} 0 & 0 \\ 1 & 5 \\ 2 & 2 \\ 3 & 7 \\ 4 & 4 \\ 5 & 1 \\ 6 & 6 \\ 7 & 3 \end{bmatrix} \qquad F = E + [0\ 4] = \begin{bmatrix} 0 & 4 \\ 1 & 1 \\ 2 & 6 \\ 3 & 3 \\ 4 & 0 \\ 5 & 5 \\ 6 & 2 \\ 7 & 7 \end{bmatrix}$$

$$G = E + [0\ 2] = \begin{bmatrix} 0 & 2 \\ 1 & 7 \\ 2 & 4 \\ 3 & 1 \\ 4 & 6 \\ 5 & 3 \\ 6 & 0 \\ 7 & 5 \end{bmatrix} \qquad H = E + [2\ 0] = \begin{bmatrix} 2 & 0 \\ 3 & 5 \\ 4 & 2 \\ 5 & 7 \\ 6 & 4 \\ 7 & 1 \\ 0 & 6 \\ 1 & 3 \end{bmatrix} \tag{39}$$

First of all, we note that all of the parallel paths have a distinct pair of 8PSK symbols which differ from each other in <u>both</u> symbol positions. Thus, in so far as single branch error events are concerned, the number of 8PSK symbols wth zero Euclidean distance from the correct path is two. Second, for an error event of length two branches, there are at least two out of the possible four 8PSK symbols that have non-zero Euclidean distance from the correct path. This is true for each of the 64 such possible paths. Finally, then, in accordance with the previous definition of L, the length of the shortest error event path is two, i.e., the asymptotic average bit error probability performance of this coded modulation scheme will vary inversely with the <u>square</u> of $\bar{E}_s/N_0$ as desired. As a specific demonstration of this result, consider again the case of coherent detection with ideal CSI. If we arbitrarily take the all zeros path as being the correct one, then, for the two branch error event, the one parallel path in F that differs by one symbol from the correct path is [0 4] (or [4 0]), which has squared Euclidean distance 4. Similarly, the one parallel path in G that differs by one symbol from the correct path is [0 2] (or [2 0]), which has squared Euclidean distance 2. For the one branch paths in parallel with [0 0], the smallest squared Euclidean distances occur for path [1 5], i.e., $4\sin^2(\pi/8)$ and $4\sin^2(5\pi/8)$ whose product is less than (4)(2) = 8. Thus, the dominant term in (9) will correspond to the one branch error event, i.e., a parallel path, for which the average bit error probability is asymptotically approximated by

$$P_b \cong \frac{1}{4}\left(\frac{4\ (1+K)}{\frac{\bar{E}_s}{N_0}}\ e^{-K}\right)^2 \frac{1}{\left(4\sin^2\left(\frac{\pi}{8}\right)\right)\left(4\sin^2\left(\frac{5\pi}{8}\right)\right)}$$

$$= \frac{1}{2} \frac{(1 + K)^2}{\left(\frac{\bar{E}_b}{N_0}\right)^2} e^{-2K} \tag{40}$$

It goes without saying that the signal sets assigned to the trellis of Figure 5 will not produce optimum performance on the AWGN channel. We now investigate the extent to which that performance is degraded relative to the optimum assignment for the AWGN illustrated in Figure 6 (see [2], Figure 4a). Since on the AWGN channel asymptotic bit error probability performance is measured by the free distance of the trellis code, we shall now compare this quantity for the trellis diagrams of Figure 5 and 6.

From Table 1 of [3], we find that $d^2_{free} = 4 \sin^2(\pi/4) + 8 \sin^2(\pi/8) = 3.172$ for the trellis code of Figure 6. The minimum Euclidean distance path for the trellis of Figure 5 also has length two branches. Then, since the minimum squared Euclidean distance between sets E and F and between sets E and G is $2(4 \sin^2(\pi/8)) = 1.1715$, we have that $d^2_{free} = 2(1.1715) = 2.343$ or a penalty of $10 \log_{10}(3.172/2.343) = 1.315$ dB.

As a second example, consider a 4 state, rate 4/5 multiple (k = 2) trellis code whose 5 output symbols are mapped into one QPSK symbol and one 8PSK symbol in each transmission interval in accordance with the generalized MTCM transmitter of Figure 1. The advantage of such a hybrid MTCM scheme over one whose multiple output symbols <u>all</u> come from the same alphabet is that the former is much less sensitive to carrier synchronization errors at the receiver. This stems from the fact that signal points in a QPSK constellation have greater distance between them than those in an 8PSK constellation and are thus less sensitive to phase jitter. Thus, one can derive the carrier reference necessary for coherent demodulation from only the received QPSK symbols. Potentially then, one can obtain an overall improvement in average system bit error probability performance relative to a 4 state, rate 4/6 (= 2/3) coded 8PSK system also of multiplicity k = 2 and throughput 2 bps/Hz, despite the fact that the latter would perform better in an ideal (perfect carrier synchronization) environment.

Figure 7 is an illustration of the trellis for the above hybrid scheme. Since $b = 4$, there are $2^b = 16$ paths emanating from each node. Thus with 4 states, we assign 4 parallel paths between nodes and the trellis is fully connected. The construction of the signal sets for assignment to the branches of this trellis which produce optimum performance on the Rician fading channel is given below:

$$A = \begin{bmatrix} 0 & 0 \\ 4 & 4 \end{bmatrix} \qquad B = \begin{bmatrix} 0 & 0 \\ 4 & 4 \end{bmatrix} + [2\ 2] = \begin{bmatrix} 2 & 2 \\ 6 & 6 \end{bmatrix}$$

$$C = A \cup B = \begin{bmatrix} 0 & 0 \\ 2 & 2 \\ 4 & 4 \\ 6 & 6 \end{bmatrix} \qquad D = C + [0\ 4] = \begin{bmatrix} 0 & 4 \\ 2 & 6 \\ 4 & 0 \\ 6 & 2 \end{bmatrix}$$

$$E = C + [0\ 2] = \begin{bmatrix} 0 & 2 \\ 2 & 4 \\ 4 & 6 \\ 6 & 0 \end{bmatrix} \qquad F = C + [0\ 6] = \begin{bmatrix} 0 & 6 \\ 2 & 0 \\ 4 & 2 \\ 6 & 4 \end{bmatrix}$$

$$G = C + [0\ 1] = \begin{bmatrix} 0 & 1 \\ 2 & 3 \\ 4 & 5 \\ 6 & 7 \end{bmatrix} \qquad H = D + [0\ 1] = \begin{bmatrix} 0 & 5 \\ 2 & 7 \\ 4 & 1 \\ 6 & 3 \end{bmatrix}$$

$$I = E + [0\ 1] = \begin{bmatrix} 0 & 3 \\ 2 & 5 \\ 4 & 7 \\ 6 & 1 \end{bmatrix} \qquad J = F + [0\ 1] = \begin{bmatrix} 0 & 7 \\ 2 & 1 \\ 4 & 3 \\ 6 & 5 \end{bmatrix} \qquad (41)$$

For the above set assignment, the error event path with the shortest length is the parallel path. Since for each set of parallel paths, both symbol positions represent distinct assignments, i.e., nonzero Euclidean distance, then the length of this one branch path is $L = 2$ symbols and, from (10), the asymptotic behavior of the average bit error probability on the Rician fading channel varies as the inverse <u>square</u> of $\bar{E}_s/N_0$. The minimum squared distance between the parallel paths is 4. However, the three branch error event path with signal set assignments, E, C, and G (see Figure 7) has a smaller squared distance equal to $2 + 0 + 4 \sin^2(\pi/8) = 2.586$ and thus we have $d^2_{free} = 2.586$.

In [6], Ungerboeck considered a 4 state, rate 2/3 conventional (k = 1) trellis coded 8PSK system with 2 parallel paths between nodes (i.e., a half-connected trellis). For his scheme, the parallel paths represented the minimum distance error event and it was found that $d^2_{free} = 4$. However, because of the absence of multiplicity, if this code were used on the fading channel, it would have an asymptotic error probability performance that varied only inverse linearly with $\bar{E}_s/N_0$. Thus, with the above hybrid MTCM scheme, we obtain a performance on the ideal AWGN channel inferior to that of the equivalent Ungerboeck code, with much improved performance on the fading channel and perhaps equivalent performance in the presence of imperfect carrier synchronization.

Set Partitioning for Multiple Trellis Coded MPSK

With the previous examples as a basis, we now describe a set partitioning method for the design of multiple trellis coded MPSK to achieve optimum performance on the Rician fading channel. In [7], Ungerboeck presented a set partitioning method for multiple trellis coding on AWGN channels. The method, which makes use of k-fold (recall that k denotes the multiplicity) Cartesian products of the sets found in Ungerboeck's original set partitioning method for conventional (k=1) trellis codes [6], is in essence the k-dimensional generalization of the latter. Since, as we have already observed, the criteria for designing optimum trellis codes on the fading channel are quite different from that for the AWGN channel (i.e., maximize d_{free}), one might anticipate that the set partitioning method would also be significantly different than that discussed in [7]. Indeed such is the case with the only common thread between the two being that we start the procedure with a k-fold Cartesian product of the complete MPSK signal set. The remainder of the procedure, along with the motivation for it, is described in what follows. For simplicity of explanation, we shall first focus our attention on the multiplicity 2 case.

Let A_0 denote the complete MPSK signal set (i.e, signal points 0,1,2,...,M-1) and $A_0 \circledast A_0$ denote a 2-fold Cartesian product of A_0 with itself. Thus, an element of the set $A_0 \circledast A_0$ is a 2-tuple whose first and second symbols are each chosen from the set A_0. The first step is to partition $A_0 \circledast A_0$ into M signal sets defined by the ordered Cartesian

product* $A_0 \textcircled{x} B_i$; i = 0,1,2,...M-1 where the jth element (j = 0,1,2,...,M-1) of B_i is defined by nj+i and the addition is performed modulo M. Thus, the jth 2-tuple from the product $A_0 \textcircled{x} B_i$ is the ordered pair (j,nj+i). The selection of the odd integer multiplier n is the key to the set partitioning method. Before presenting the relation whose solution provides the desired value(s) of n, we shall first discuss what the first partitioning step is trying to accomplish.

The first partitioning step accomplishes two purposes. First it guarantees that within any of the M partitions, each of the two symbol positions has distinct elements. That is to say, for any 2-tuple within a partitioned set, the Euclidean distance of each of the two symbols from the corresponding symbols in any other 2-tuple within the same set is nonzero. We recall that this is the desired property from the standpoint of maximizing the "length" of the shortest error event path. Stated another way, if the shortest error path is of length 1 branch (i.e., parallel paths exist in the trellis and have the smallest Euclidean distance from the correct path), then the length L of this path is guaranteed to have value 2 and the error probability performance on the fading channel will vary as the inverse square of $\bar{E}_s/N_0$.

The second purpose accomplished is that the minimum Euclidean distance <u>product</u> between 2-tuples within a partitioned set, i.e., the minimum of the product of the distances between corresponding symbol positions of all pairs of 2-tuples, is maximized. To determine the value of this distance, we observe that the set B_i+1 is merely a cyclic shift of the set B_i, i.e., a clockwise rotation of the corresponding signal points by an angle $2\pi/M$. Thus, since the squared Euclidean distance between a pair of 2-tuples is the sum of the squared Euclidean distances between corresponding symbols in the 2-tuples, the above set partitioning guarantees that the <u>intra</u>distance structure of all of the partitions $A_0 \textcircled{x} B_i$ is <u>identical</u>. Thus, it is sufficient to study the distance structure of $A_0 \textcircled{x} B_0$, henceforth called the <u>generating set</u>. For this set, the product of the squared distances between the ith 2-tuple and the jth 2-tuple is

*By ordered Cartesian product we mean the concatenation of corresponding elements in the two sets forming the product.

$$\Pi d_{ij}^2 = \left(4 \sin^2\left(\frac{(j-i)\pi}{M}\right)\right)\left(4 \sin^2\left(\frac{n(j-i)\pi}{M}\right)\right) \tag{42}$$

Thus, based on the above requirement, we wish to choose n such that the minimum of Πd_{ij}^2 over all pairs of 2-tuples in $A_0 \textcircled{x} B_0$ is maximized. Making use of the symmetry properties of the MPSK signaling set around the circle, we can write the above as follows. Letting n* denote the desired value(s) of n, then n* has the maximin solution(s).

$$f(n^*) = \max_{n^*=1,3,5,\ldots,M/2-1} \min_{m=1,2,\ldots,M/2-1} 16 \sin^2\left(\frac{m\pi}{M}\right)\sin^2\left(\frac{n^*m\pi}{M}\right) \tag{43a}$$

Equation (43a) has the equivalent vector form

$$g(n^*) = \max_{n^*=1,3,5,\ldots,M/2-1} \min_{m=1,2,\ldots,M/2-1} |z^m - 1|^2 \, |z^{n^*m}-1|^2 \tag{43b}$$

where $z = \exp(j2\pi/M)$ represents a unit vector with phase equal to that between adjacent points in the signal constellation. For M=2, we have the degenerate solution n*=1.

Note that the additive inverse(s) of n*, i.e., M-n* is (are) also valid solutions. This conclusion is easily derived by substituting $z^{M-n} = \exp(j2\pi(M-n)/M) = z^{-n}$ for z^n in (43b) and observing that the equation is unchanged.

Table 1 gives the solution of (43) for M=4, 8, 16, 32, and 64.

The sets obtained by this first partition are illustrated below for the case M=8 and n*=3 which is the single solution of (43). (Note that the additive inverse n*=5 could also have been used to generate (44).)

$$A_0 \circledast B_0 = \begin{bmatrix} 0 & 0 \\ 1 & 3 \\ 2 & 6 \\ 3 & 1 \\ 4 & 4 \\ 5 & 7 \\ 6 & 2 \\ 7 & 5 \end{bmatrix} \quad A_0 \circledast B_1 = \begin{bmatrix} 0 & 1 \\ 1 & 4 \\ 2 & 7 \\ 3 & 2 \\ 4 & 5 \\ 5 & 0 \\ 6 & 3 \\ 7 & 6 \end{bmatrix} \quad A_0 \circledast B_2 = \begin{bmatrix} 0 & 2 \\ 1 & 5 \\ 2 & 0 \\ 3 & 3 \\ 4 & 6 \\ 5 & 1 \\ 6 & 4 \\ 7 & 7 \end{bmatrix} \quad A_0 \circledast B_3 = \begin{bmatrix} 0 & 3 \\ 1 & 6 \\ 2 & 1 \\ 3 & 4 \\ 4 & 7 \\ 5 & 2 \\ 6 & 5 \\ 7 & 0 \end{bmatrix}$$

$$A_0 \circledast B_4 = \begin{bmatrix} 0 & 4 \\ 1 & 7 \\ 2 & 2 \\ 3 & 5 \\ 4 & 0 \\ 5 & 3 \\ 6 & 6 \\ 7 & 1 \end{bmatrix} \quad A_0 \circledast B_5 = \begin{bmatrix} 0 & 5 \\ 1 & 0 \\ 2 & 3 \\ 3 & 6 \\ 4 & 1 \\ 5 & 4 \\ 6 & 7 \\ 7 & 2 \end{bmatrix} \quad A_0 \circledast B_6 = \begin{bmatrix} 0 & 6 \\ 1 & 1 \\ 2 & 4 \\ 3 & 7 \\ 4 & 2 \\ 5 & 5 \\ 6 & 0 \\ 7 & 3 \end{bmatrix} \quad A_0 \circledast B_7 = \begin{bmatrix} 0 & 7 \\ 1 & 2 \\ 2 & 5 \\ 3 & 0 \\ 4 & 3 \\ 5 & 6 \\ 6 & 1 \\ 7 & 4 \end{bmatrix} \qquad (44)$$

Note that sets $A_0 \circledast B_0$, $A_0 \circledast B_2$, $A_0 \circledast B_4$, $A_0 \circledast B_6$ of (44), which have the largest distance between them, i.e., the largest interdistance, are identical, respectively, to sets E, G, F, and H in Figure 5, where only 4 sets of 8 elements each were needed and $n^*=5$ rather than $n^*=3$ was used. Equivalently, one could have employed sets $A_0 \circledast B_1$, $A_0 \circledast B_3$, $A_0 \circledast B_5$, and $A_0 \circledast B_7$ in Figure 5.

If one was to follow tradition, then the second step in the set partitioning procedure would be to partition each of the M sets $A_0 \circledast B_i$; $i=0,1,2,\ldots,M-1$, as in (44), for example, into two sets $C_0 \circledast D_{i0}$ and $C_1 \circledast D_{i1}$, with the first containing the even elements ($j=0,2,4,\ldots,M-2$) and the second containing the odd elements ($j=1,3,5,\ldots,M-1$). While it is true that for each of these partitioned sets, the elements in each of the two symbol positions would still be distinct, unfortunately, it is not always true that these sets have the minimum Euclidean product distance between 2-tuples maximized. Thus, we immediately conclude that the appropriate method to generate the sets on the second level of partition does not necessarily follow a tree structure.

After a little thought, it becomes obvious that one should partition in such a way that the resulting sets (of dimensionality M/2) should have an intradistance product structure equal to that which would be achieved by a first level partitioning in accordance with (43) with, however, M replaced by M/2. Interestingly enough, this second level of set partitioning

can still be achieved by an odd-even split of a first level partitioning like that previously described; however, the value of n* used to generate the sets on this first level should be that corresponding to the solution of (43) with M replaced by M/2 (or its additive inverse). Note that if one of the solutions of (43) (including the additive inverse) is equal to one of the solutions of (43) (again including the additive inverses) when M is replaced by M/2, then indeed the first two levels of set partitioning follow a <u>tree structure</u>. By inspection of Table 1, we observe that when M=4, 8, and 32, there exists a value of n* common to these values of M and the corresponding values of M/2. Thus, for M=4, 8, and 32 the first two levels of set partitioning follow a tree structure whereas, for M=16, they do not.

As an example of the second level of set partitioning, the sets that result from the partitioning of the sets in (44) are given below

$$C_0 \circledast D_{00} = \begin{bmatrix} 0 & 0 \\ 2 & 6 \\ 4 & 4 \\ 6 & 2 \end{bmatrix} \quad C_j \circledast D_{01} = \begin{bmatrix} 1 & 3 \\ 3 & 1 \\ 5 & 7 \\ 7 & 5 \end{bmatrix} \quad C_0 \circledast D_{10} = \begin{bmatrix} 0 & 1 \\ 2 & 7 \\ 4 & 5 \\ 6 & 3 \end{bmatrix} \quad C_1 \circledast D_{11} = \begin{bmatrix} 1 & 4 \\ 3 & 2 \\ 5 & 0 \\ 7 & 6 \end{bmatrix}$$

$$C_0 \circledast D_{20} = \begin{bmatrix} 0 & 2 \\ 2 & 0 \\ 4 & 6 \\ 6 & 4 \end{bmatrix} \quad C_1 \circledast D_{21} = \begin{bmatrix} 1 & 5 \\ 3 & 3 \\ 5 & 1 \\ 7 & 7 \end{bmatrix} \quad C_0 \circledast D_{30} = \begin{bmatrix} 0 & 3 \\ 2 & 1 \\ 4 & 7 \\ 6 & 5 \end{bmatrix} \quad C_1 \circledast D_{31} = \begin{bmatrix} 1 & 6 \\ 3 & 4 \\ 5 & 2 \\ 7 & 0 \end{bmatrix}$$

$$C_0 \circledast D_{40} = \begin{bmatrix} 0 & 4 \\ 2 & 2 \\ 4 & 0 \\ 6 & 6 \end{bmatrix} \quad C_1 \circledast D_{41} = \begin{bmatrix} 1 & 7 \\ 3 & 5 \\ 5 & 3 \\ 7 & 1 \end{bmatrix} \quad C_0 \circledast D_{50} = \begin{bmatrix} 0 & 5 \\ 2 & 3 \\ 4 & 1 \\ 6 & 7 \end{bmatrix} \quad C_1 \circledast D_{51} = \begin{bmatrix} 1 & 0 \\ 3 & 6 \\ 5 & 4 \\ 7 & 2 \end{bmatrix}$$

$$C_0 \circledast D_{60} = \begin{bmatrix} 0 & 6 \\ 2 & 4 \\ 4 & 2 \\ 6 & 0 \end{bmatrix} \quad C_1 \circledast D_{61} = \begin{bmatrix} 1 & 1 \\ 3 & 3 \\ 5 & 5 \\ 7 & 3 \end{bmatrix} \quad C_0 \circledast D_{70} = \begin{bmatrix} 0 & 7 \\ 2 & 5 \\ 4 & 3 \\ 6 & 1 \end{bmatrix} \quad C_1 \circledast D_{71} = \begin{bmatrix} 1 & 2 \\ 3 & 0 \\ 5 & 6 \\ 7 & 4 \end{bmatrix} \qquad (45)$$

and the corresponding tree structure is illustrated in Figure 8.

The third and succeeding steps are identical in construction to the second step, namely, we partition each set on the present level into two sets containing the alternate rows with the sets for the present level determined by a value of n* computed from (43) with M successively replaced by M/4, M/8, etc.

To extend the previous procedure to higher multiplicity of order $k \geq 2$, we can simply form the k/2-fold ordered Cartesian product of all the sets on a given partition level created by the procedure for k=2. The result of this procedure is illustrated in Figure 9 for k=4. If the number of sets required to satisfy the trellis is less than the number of sets generated on a particular partition level, then one would choose those that have largest interdistance, as was done in the example of Figure 5. Also, as for the k=2 case, the sets formed by this generalized set partitioning procedure will all have distinct elements in any of the k symbol positions. Thus, the length of a 1 branch error event path will have value k, and hence the asymptotic bit error rate performance of such a trellis code on the fading channel will vary inversely with $(\bar{E}_s/N_0)^n$ with $n \geq k$. Thus we can conclude that in so far as the rate of decay of average bit error probability with $\bar{E}_s/N_0$ is concerned, incorporating multiplicity in the design of the trellis code has a similar effect to using diversity, a technique commonly employed to improve performance on fading channels.

A more optimum procedure for k>2 would be to generalize (43b) to

$$g(n_1^*, n_2^*, \ldots, n_{k-1}^*) = \max_{n_1^*, n_2^*, \ldots, n_{k-1}^* = 1,3,5,\ldots,M/2-1} \; \min_{m=0,1,2,\ldots,M/2-1} |z^m - 1|^2 \prod_{i=1}^{k-1} |z^{n_i^* m} - 1|^2 \qquad (46)$$

The set of maximum solutions $n_1^*, n_2^*, \ldots, n_{k-1}^*$ can be used to produce all of the necessary sets on any level of partition.

More Examples

1. 4 State Rate 4/6 Trellis Coded 8PSK

Consider a 4 state rate 4/6 trellis coded 8PSK system designed for optimum performance on the Rician fading channel. The trellis diagram appears as in Figure 7, where the signal point sets assigned to the branches are derived from the previous procedure and are given by

$$C = \begin{bmatrix} 00 \\ 22 \\ 44 \\ 66 \end{bmatrix} \quad D = \begin{bmatrix} 15 \\ 37 \\ 51 \\ 73 \end{bmatrix} \quad E = \begin{bmatrix} 04 \\ 26 \\ 40 \\ 62 \end{bmatrix} \quad F = \begin{bmatrix} 11 \\ 33 \\ 55 \\ 77 \end{bmatrix}$$

$$G = \begin{bmatrix} 02 \\ 24 \\ 46 \\ 60 \end{bmatrix} \quad H = \begin{bmatrix} 17 \\ 31 \\ 53 \\ 75 \end{bmatrix} \quad I = \begin{bmatrix} 06 \\ 20 \\ 42 \\ 64 \end{bmatrix} \quad J = \begin{bmatrix} 13 \\ 35 \\ 57 \\ 71 \end{bmatrix} \tag{47}$$

For this assignment, each set has a minimum squared intradistance 4 + 4 = 8, which represents the minimum square Euclidean distance between parallel paths. Each of these one branch paths when viewed as an error event path has a length L=2 with respect to any of the other paths in parallel with it. Every other error event path (consisting of two or more branches) has a length L greater than two regardless of which path is chosen as the correct path. Thus, the dominant term in the asymptotic bit error probability expression of (9) corresponds once again to the parallel paths. Since the minimum squared intradistance for each of the two symbols in any of these 2-tuples is 4, then analogous to (40), which describes the performance of the same scheme using only a 2 state trellis, we get

$$P_b \cong \frac{1}{4}\left(\frac{4(1+K)}{\frac{\bar{E}_s}{N_0}}\, e^{-K}\right)^2 \frac{1}{(4)(4)}$$

$$= \frac{1}{16}\,\frac{(1+K)^2}{\left(\frac{\bar{E}_b}{N_0}\right)^2}\, e^{-2K} \tag{48}$$

i.e., a gain of 4.5 dB in SNR.

2. 2 State Rate 4/12 Trellis Coded 8PSK

This is an example of a multiplicity 4 trellis code optimally designed for the Rician fading channel. Since 4 8PSK symbols are transmitted over the channel for each 4 bits into the encoder, the throughput of the code is 1 bps/Hz. The state diagram is as in Figure 5, where E, F, G, and H are chosen as those sets

which have largest interdistance in the construction of Figure 9. As such, we have

$$E = A_0 \circledast B_0 \circledast A_0 \circledast B_0 = \begin{bmatrix} 0 & 0 & 0 & 0 \\ 1 & 5 & 1 & 5 \\ 2 & 2 & 2 & 2 \\ 3 & 7 & 3 & 7 \\ 4 & 4 & 4 & 4 \\ 5 & 1 & 5 & 1 \\ 6 & 6 & 6 & 6 \\ 7 & 3 & 7 & 3 \end{bmatrix} \qquad F = A_0 \circledast B_4 \circledast A_0 \circledast B_4 = \begin{bmatrix} 0 & 4 & 0 & 4 \\ 1 & 1 & 1 & 1 \\ 2 & 6 & 2 & 6 \\ 3 & 3 & 3 & 3 \\ 4 & 0 & 4 & 0 \\ 5 & 5 & 5 & 5 \\ 6 & 2 & 6 & 2 \\ 7 & 7 & 7 & 7 \end{bmatrix}$$

$$G = A_0 \circledast B_2 \circledast A_0 \circledast B_2 = \begin{bmatrix} 0 & 2 & 0 & 2 \\ 1 & 7 & 1 & 7 \\ 2 & 4 & 2 & 4 \\ 3 & 1 & 3 & 1 \\ 4 & 6 & 4 & 6 \\ 5 & 3 & 5 & 3 \\ 6 & 0 & 6 & 0 \\ 7 & 5 & 7 & 5 \end{bmatrix} \qquad H = A_0 \circledast B_6 \circledast A_0 \circledast B_6 = \begin{bmatrix} 0 & 6 & 0 & 6 \\ 1 & 3 & 1 & 3 \\ 2 & 0 & 2 & 0 \\ 3 & 5 & 3 & 5 \\ 4 & 2 & 4 & 2 \\ 5 & 7 & 5 & 7 \\ 6 & 4 & 6 & 4 \\ 7 & 1 & 7 & 1 \end{bmatrix} \tag{49}$$

For this code all sets have squared Euclidean intradistance equal to 8. The asymptotic average bit error probability for coherent detection with ideal CSI is computed analogous to (40) and is given by

$$P_b \cong \frac{1}{4}\left(\frac{4(1+K)}{\frac{\bar{E}_s}{N_0}}\, e^{-K}\right)^4 \frac{1}{\left(4\sin^2\left(\frac{\pi}{8}\right)\right)^2 \left(4\sin^2\left(\frac{5\pi}{8}\right)\right)^2}$$

$$= \frac{(1+K)^4 e^{-4K}}{\left(\frac{\bar{E}_b}{N_0}\right)^4} \tag{50}$$

Note that because the multiplicity is equal to 4, the average bit error probability of (4) varies inversely with $(\bar{E}_b/N_0)4$, where now $\bar{E}_s = \bar{E}_b$.

3. 4 State Rate 5/6 Trellis Coded 8PSK

This is an example of a multiplicity 2 trellis code with noninteger throughput (i.e., 2.5) optimally designed for the Rician fading channel. The trellis diagram is as in Figure 5 with the following set assignments:

$$
\begin{aligned}
C &= A_0 \textcircled{x} B_0 & D &= A_0 \textcircled{x} B_2 \\
E &= A_0 \textcircled{x} B_4 & F &= A_0 \textcircled{x} B_6 \\
G &= A_0 \textcircled{x} B_1 & H &= A_0 \textcircled{x} B_3 \\
I &= A_0 \textcircled{x} B_5 & J &= A_0 \textcircled{x} B_7
\end{aligned}
\tag{51}
$$

where the sets $A_0 \textcircled{x} B_i$; i = 0,1,2...,7 are as in (44). Again we remind the reader that n* = 5 rather than n* = 3 could have been used to generate these sets. By construction, the parallel paths in each of the above sets have length L=2. Also, the minimum square Euclidean distance product for these parallel paths is $\Pi d^2 = (4 \sin^2(\pi/8)) \times (4 \sin^2(5\pi/8)) = 2$. If we examine all of the two branch error event paths, we find that the shortest length of these paths is also L=2. The minimum squared Euclidean distance product for these two branch paths is $(4 \sin^2 2(\pi/8)) \times (4 \sin^2(\pi/8)) = 1.172$, which is smaller than 2 and thus dominates the asymptotic error probability performance. In particular, for coherent detection with ideal CSI, we have that

$$
P_b \cong \frac{1}{5} \left(\frac{4(1+K)e^{-K}}{\frac{\bar{E}_s}{N_0}} \right)^2 \frac{1}{1.172} = 0.437 \; \frac{(1+K)^2}{\left(\frac{\bar{E}_b}{N_0}\right)^2} e^{-2K} \tag{52}
$$

where $\bar{E}_s = 2.5\ \bar{E}_b$.

The squared free distance of this code is determined by the error event path of length three branches indicated in Figure 5 and is given by $d^2_{free} = 2(4 \sin^2(\pi/8)) + 4 \sin^2(\pi/8) = 1.757$. The equivalent code optimized for the AWGN [8] has $d^2_{free} = 2$ but only L=1.

4. 8 State Rate 3/6 Trellis Coded 8PSK

The last example is another one with noninteger throughput (i.e., 1.5). Also, since there are $2^3 = 8$ branches emanating from each node and the trellis has 8 states, there are no parallel paths and the trellis is fully connected. The trellis diagram is illustrated in Figure 10 with the following set assignments:

$$A^{(0)} = A_0 \textcircled{x} B_0$$
$$B^{(0)} = A_0 \textcircled{x} B_4 \qquad (53)$$

Also $A^{(i)}$ and $B^{(i)}$; i = 1,2,3 are cyclic shifts of $A^{(0)}$ and $B^{(0)}$, respectively, by i rows. This code achieves a minimum diversity L=3 corresponding to an error event path of length 2 branches. Also, the minimum product of squared Euclidean distances is given by $\Pi d^2 = (4 \sin^2(\pi/8))$ x $(4 \sin^2(5\pi/8))$ x 4 = 8, which corresponds to the error event path (relative to the all zeros path) with 8PSK symbols (1,3) and (0,4) along its branches. Finally then, the bit error probability is asymptotically approximated by

$$P_b \cong \frac{1}{3}\left(\frac{4(1+K)e^{-K}}{\frac{\bar{E}_s}{N_0}}\right)^3 \frac{1}{8} = 0.79\,\frac{(1+K)^3 e^{-3K}}{\left(\frac{\bar{E}_b}{N_0}\right)^3} \qquad (54)$$

where $\bar{E}_s/N_0 = 1.5\ \bar{E}_b/N_0$. The squared free distance is determined by the two branch path with 8PSK symbol assignments (3,1) and (1,7) and is given by $d^2_{free} = 4 \sin^2(3\pi/8) + 4 \sin^2(\pi/8) = 5.172$.

Another interesting generalization of this example is as follows. When there are no parallel paths in the trellis, as is true here, it may be desirable to go to a larger modulation constellation (e.g., 16PSK rather than 8PSK) to achieve an increase in diversity. To demonstrate this idea, consider the following set assignment to the trellis diagram of Figure 10. First construct sets $A_0 \textcircled{x} B_0$ and $A_0 \textcircled{x} B_4$ with n* = 3 and for 16PSK. Next, partition these sets in accordance with Figure 9. Now choose the sets in Figure 10 as:

$$A^{(0)} = C_0 \textcircled{x} D_{00} = \begin{bmatrix} 0 & 0 \\ 2 & 6 \\ 4 & 12 \\ 6 & 2 \\ 8 & 8 \\ 10 & 14 \\ 12 & 4 \\ 14 & 10 \end{bmatrix}; \qquad B^{(0)} = C_0 \textcircled{x} D_{41} = \begin{bmatrix} 1 & 7 \\ 3 & 13 \\ 5 & 3 \\ 7 & 9 \\ 9 & 15 \\ 11 & 5 \\ 13 & 11 \\ 15 & 1 \end{bmatrix} \qquad (55)$$

together with the appropriate cyclic shifts as before. We note that with this assignment, all of the two branch error event paths differ from the correct path in four 16PSK symbols and thus the diversity is now L=4. Unfortunately, the minimum product of squared Euclidean distances will be reduced to the value $\Pi d^2 = (4 \sin^2(2\pi/16)) \times (4 \sin^2(10\pi/16)) \times (4 \sin^2(\pi/16)) \times (4 \sin^2(9\pi/16)) = 1.172$ and thus the choice between 8PSK and 16PSK modulations depends on the value of $\bar{E}_b/N_0$ one is operating at.

REFERENCES

1. D. Divsalar and M. K. Simon, "Trellis Coded Modulation for 4800 to 9600 bps Transmission Over a Fading Satellite Channel," JPL Publication 86-8 (MSAT-X Report No. 129), June 1, 1986. Also see IEEE Journal on Selected Areas in Communications, Vol. SAC-5, No. 2, February 1987, pp. 162-175.

2. D. Divsalar and M. K. Simon, "Multiple Trellis Coded Modulation (MTCM)," JPL Publication 86-44 (MSAT-X Report No. 141), November 15, 1986. Also see IEEE Global Telecommunications Conference Record, Houston, TX, December 1-4, 1986, pp. 30.8.1 - 30.8.7.

3. M. K. Simon and D. Divsalar, "Multiple Trellis Coded Modulation (MTCM) Performance on a Fading Satellite Channel," presented at the IEEE Global Telecommunications Conference, Tokyo, Japan, November 1987.

4. M. K. Simon and D. Divsalar, "The Performance of Trellis Coded Multilevel DPSK on a Fading Mobile Satellite Channel," JPL Publication 87-8 (MSAT-X Report No. 144), June 1, 1987.

5. M. K. Simon and D. Divsalar, "Combined Trellis Coding with Asymmetric MPSK Modulation," JPL Publication 85-24 (MSAT-X Report 109), May 1, 1985. Also see IEEE Transactions on Communications, Vol. COM-35, No. 2, February 1987, pp. 130-141.

6. G. Ungerboeck, "Channel Coding with Multilevel/Phase Signals," IEEE Transactions on Information Theory, Vol. IT-28, No. 1, January 1982, pp. 55-67.

7. G. Ungerboeck, "Trellis-Coded Modulation with Redundant Signal Sets; Part I: Introduction; Part II: State of the Art," IEEE Communications Magazine, Vol. 25, No. 2, February 1987, pp. 5-21.

8. S. G. Wilson, "Rate 5/6 Trellis-Coded 8-PSK," IEEE Transactions on Communications, Vol. COM-34, No. 18, October 1986, pp. 1045-1049.

Appendix A: Proof that d^2 Defined in (5b) Satisfies the Conditions for a Distance Metric

Theorem: Let $K \geq 0$, $\gamma > 0$, and δ be a metric. Then

$$d(x,y) = \left(\frac{K\,\delta^2(x,y)}{1 + K + \gamma\,\delta^2(x,y)} + \frac{1}{\gamma} \ln \left(\frac{1 + K + \gamma\,\delta^2(x,y)}{1 + K} \right) \right)^{1/2} \tag{A-1}$$

is a metric, where

$$\delta^2(x,y) \triangleq |x-y|^2 \tag{A-2}$$

Proof:

Letting

$$\delta_0^2(x,y) = \frac{\gamma}{1+K}\,\delta^2(x,y) \tag{A-3}$$

then, we can rewrite (A-1) as

$$d(x,y) = \frac{1}{\sqrt{\gamma}} \left[\frac{K\,\delta_0^{\,2}(x,y)}{1 + \delta_0^2(x,y)} + \ln \left(1 + \delta_0^{\,2}(x,y) \right) \right]^{1/2} \tag{A-4}$$

Since multiplication of a metric by a constant does not change its metric status, it is sufficient to show that*

$$d(x,y) \triangleq \left[\frac{K\,\delta^2(x,y)}{1 + \delta^2(x,y)} + \ln \left(1 + \delta^2(x,y) \right) \right]^{1/2} \tag{A-5}$$

is a metric.

---

*For simplicity of notation, we shall drop the zero subscript on δ_0.

Consider a function $\phi(t)$ defined over the domain R^+ (the set of positive real numbers) and taking on values over R^+. Let $\phi(t)$ have the following four properties:

$$\begin{array}{ll} (1) & \phi(0) > 0 \\ (2) & \phi(t) > 0 \\ (3) & \phi'(t) > 0 \\ (4) & \phi''(t) < 0 \end{array} \qquad \text{(A-6)}$$

We shall now show that $\phi(\delta(x,y))$ is a metric. We observe that (A-6) implies that $\phi(t)$ is a monotonically increasing function with decreasing slope as t increases. From conditions (1)-(3) of (A-6), we have that (see Figure A-1)

$$\phi(t_3) < \phi(t_1+t_2) \quad \text{for } t_3 > t_1+t_2 \qquad \text{(A-7)}$$

Further imposing condition (4) of (A-6) results in

$$\frac{\phi(t_1+t_2) - \phi(t_1)}{t_2} < \phi'(t_1)$$

$$\frac{\phi(t_2)}{t_2} > \phi'(t_2) > \phi'(t_1) \qquad \text{(A-8)}$$

Combining (A-7) and (A-8), we have that

$$\phi(t_3) < \phi(t_1) + \phi(t_2) \qquad \text{(A-9)}$$

Letting

$$\begin{aligned} t_1 &= \delta(x,y) \\ t_2 &= \delta(y,z) \\ t_3 &= \delta(x,z) \end{aligned} \qquad \text{(A-10)}$$

then for the triangular inequality on δ, namely,

$$\delta(x,z) > \delta(x,y) + \delta(y,z) \tag{A-11}$$

we have from (A-9) that $\phi(\delta)$ satisfies the triangular inequality

$$\phi(\delta(x,z)) < \phi(\delta(x,y)) + \phi(\delta(y,z)) \tag{A-12}$$

and is thus a metric.

It remains to show that $\phi(\delta(x,y)) = d(x,y)$ satisfies the conditions of (A-6).

Letting

$$\phi(t) = \left[\frac{Kt^2}{1+t^2} + \ln\,(1 + t^2)\right]^{1/2} \tag{A-13}$$

we immediately observe that conditions (1) and (2) are satisfied. The first derivative of $\phi(t)$ is given by

$$\phi'(t) = \frac{t(1+K+t^2)}{\phi(t)\,(1+t^2)^2} \tag{A-14}$$

which is obviously greater than zero for all t greater than zero. (Condition (3) is satisfied.) Finally, the second derivative of $\phi(t)$ is

$$\phi''(t) = \frac{1+K-3Kt^2-t^4}{(1+t^2)^3} - \frac{1}{\phi^2(t)}\,\frac{t^2(1+K+t^2)^2}{(1+t^2)^4} \tag{A-15}$$

Since $\ln\,(1+t^2) \leq t^2$, we have from (A-13) that

$$\phi^2(t) \leq \frac{t^2(1+K+t^2)}{1+t^2} \tag{A-16}$$

Combining (A-15) and (A-16) gives

$$\phi''(t) \leq - \frac{(3K+1)t^2 + t^4}{(1+t^2)^3} \qquad \text{(A-17)}$$

which obviously satisfies condition (4). Q.E.D.

Table 1

The Solutions of Equation (43) for Various Values of M

M	n*
2	1,1
4	1,3
8	3,5
16	7,9
32	7,9,23,25
64	19,27,37,45

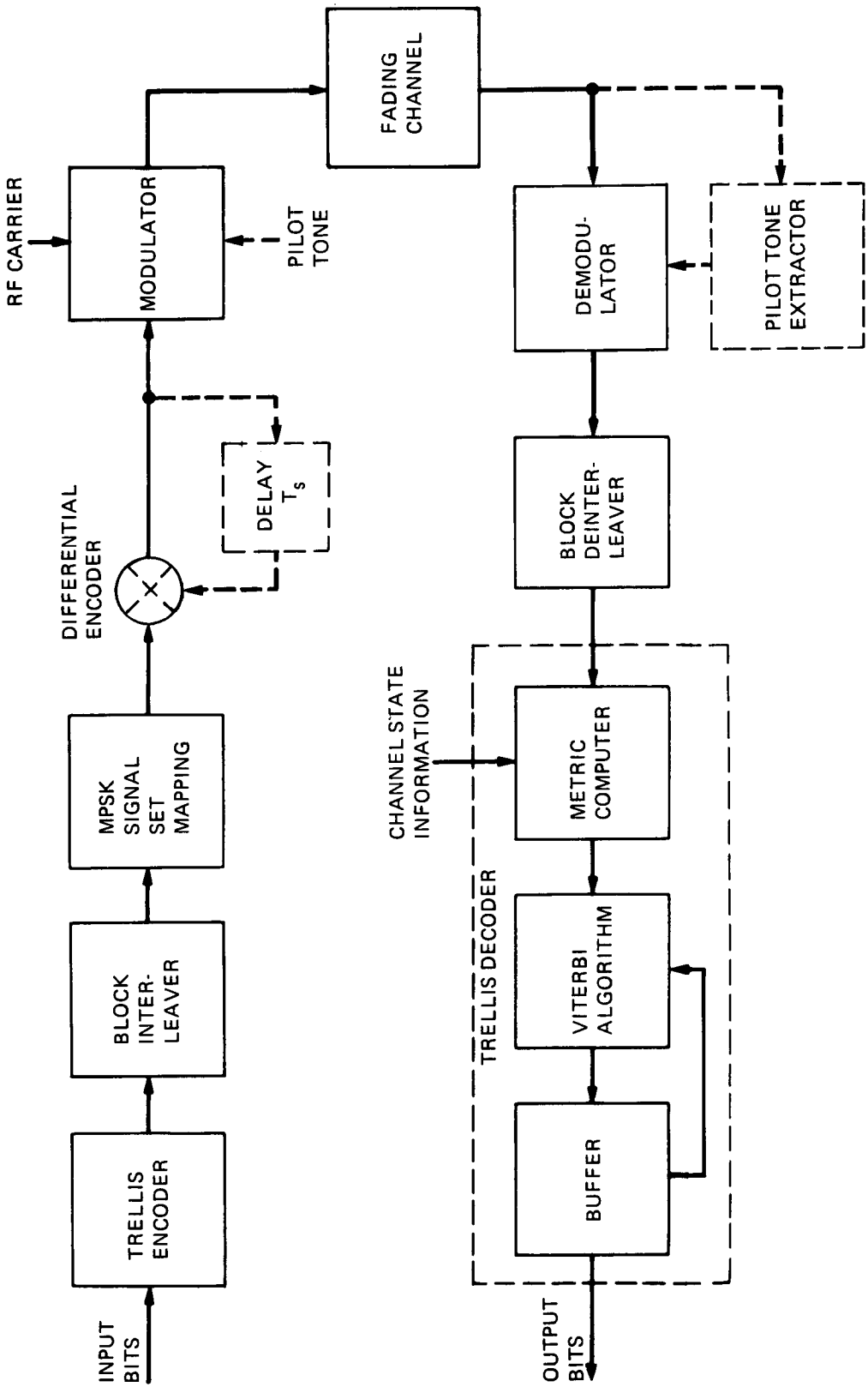

Figure 1. Block Diagram of the Trellis Coded System

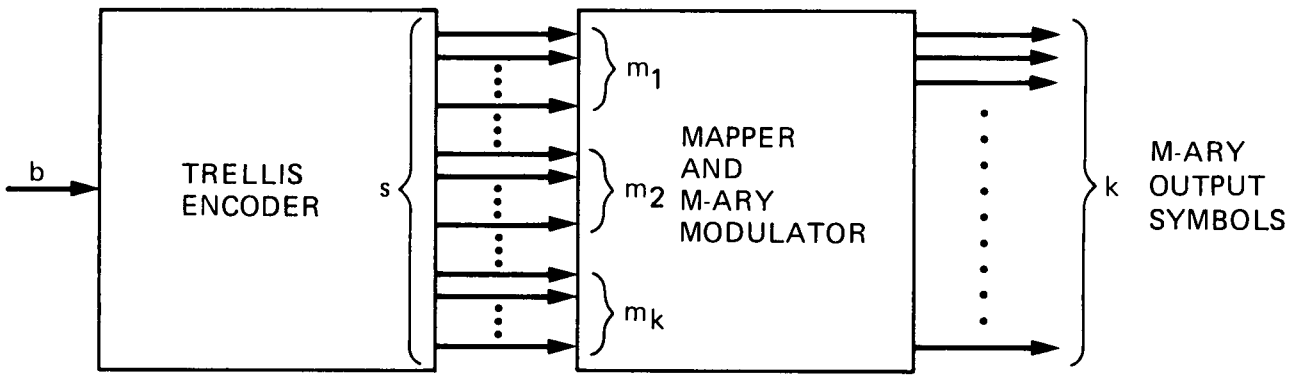

Figure 2. Multiple Trellis Encoded MPSK Transmitter

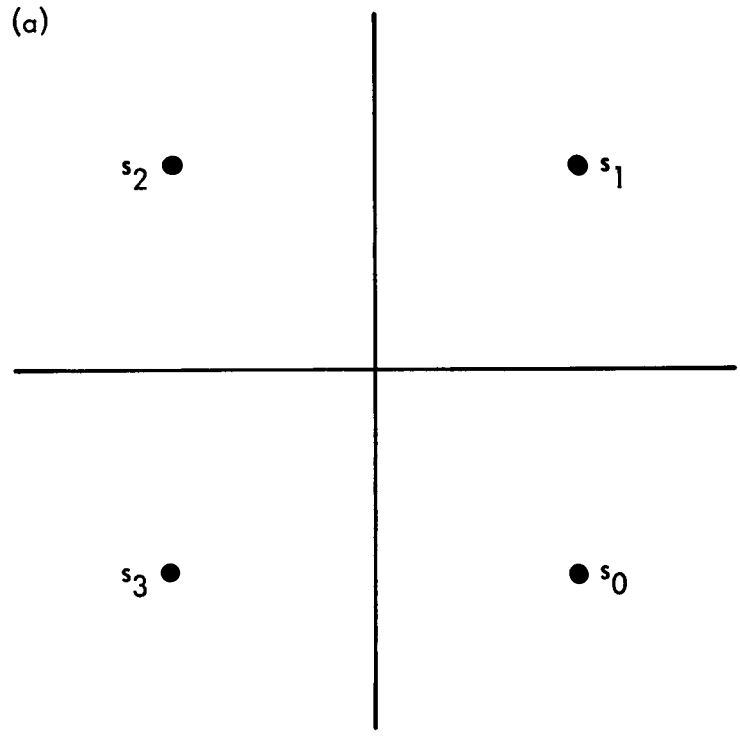

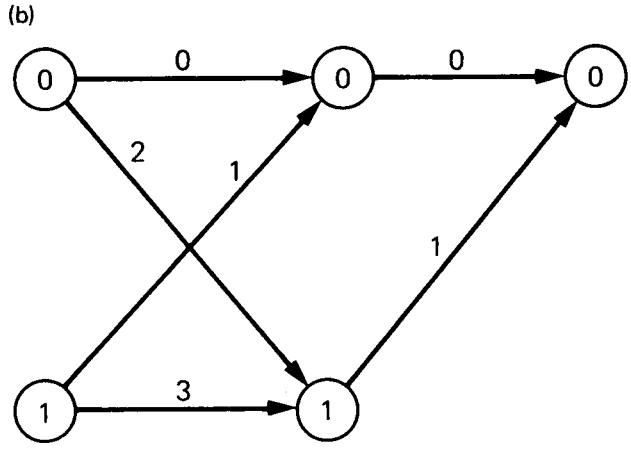

Figure 3. (a) Symmetric QPSK Signal Point Constellation, (b) Trellis Diagram for Conventional Rate 1/2 Trellis Coded QPSK

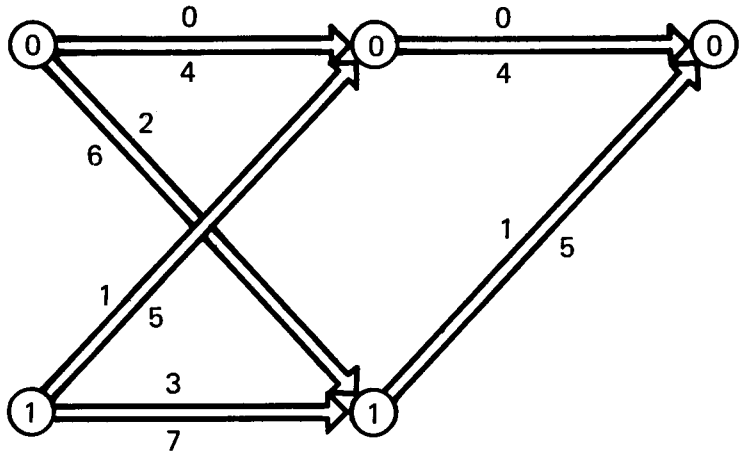

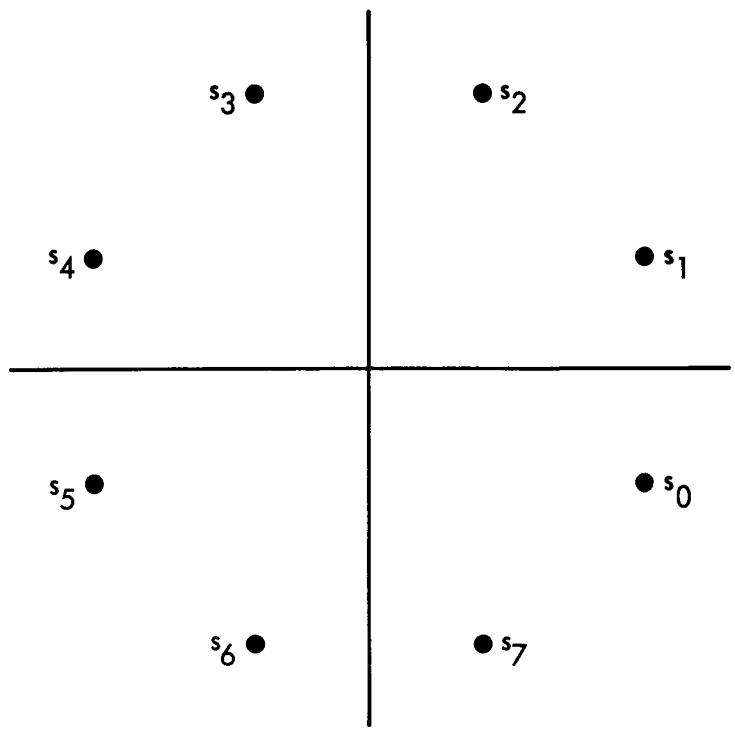

SYMMETRIC 8-PSK

Figure 4. Trellis Diagram for Conventional Rate 2/3 Coded 8PSK; 2 States

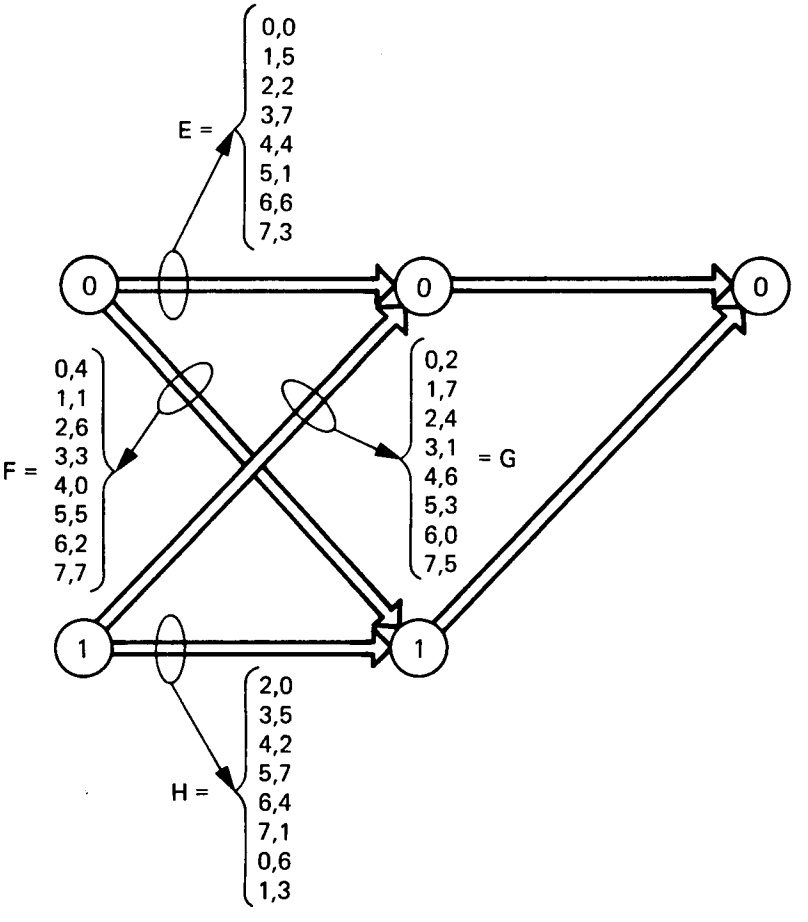

Figure 5. Trellis Diagram for Multiple (k = 2) Rate 2/3 Coded 8PSK; 2 States

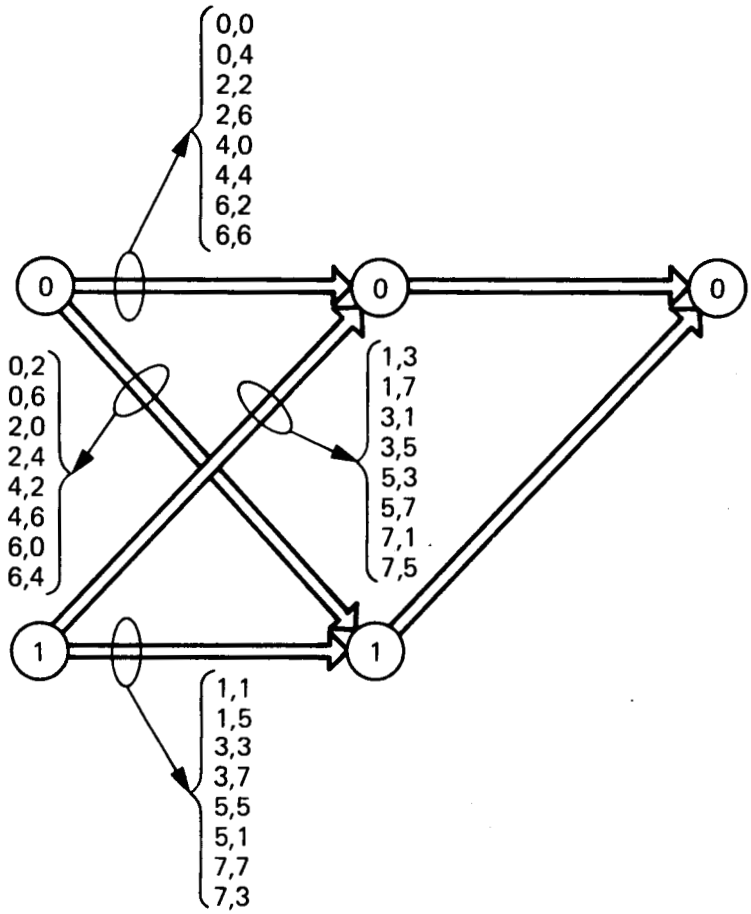

Figure 6. Trellis Diagram for Optimum Multiple (k = 2) Rate 2/3 Coded 8PSK on AWGN; 2 States

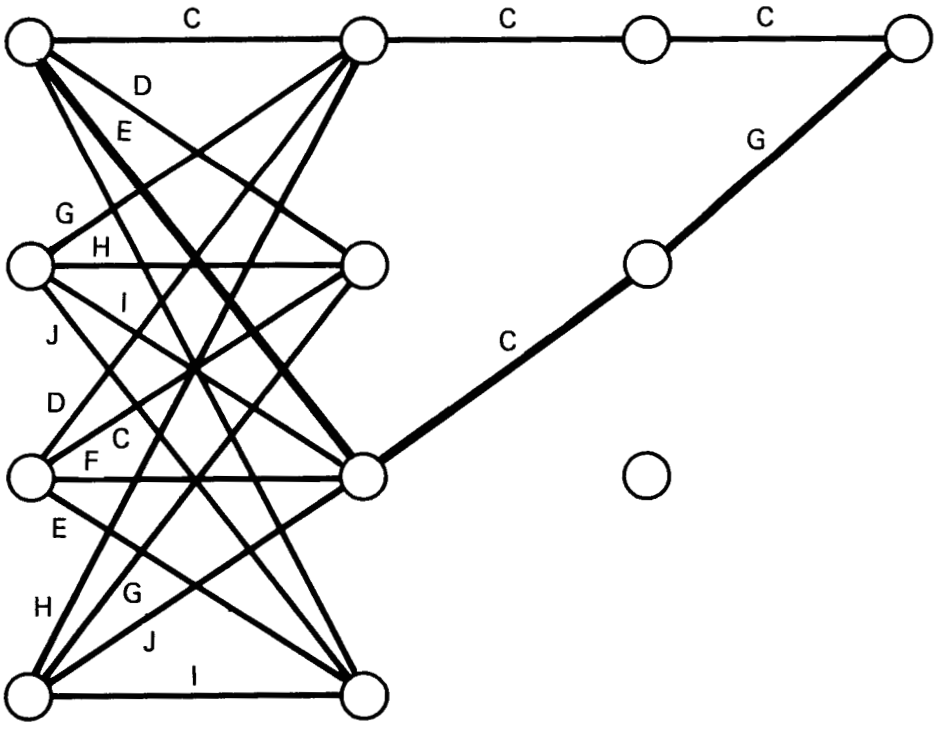

Figure 7. 4-State Trellis for Rate 4/5 Hybrid QPSK/8PSK Multiple TCM

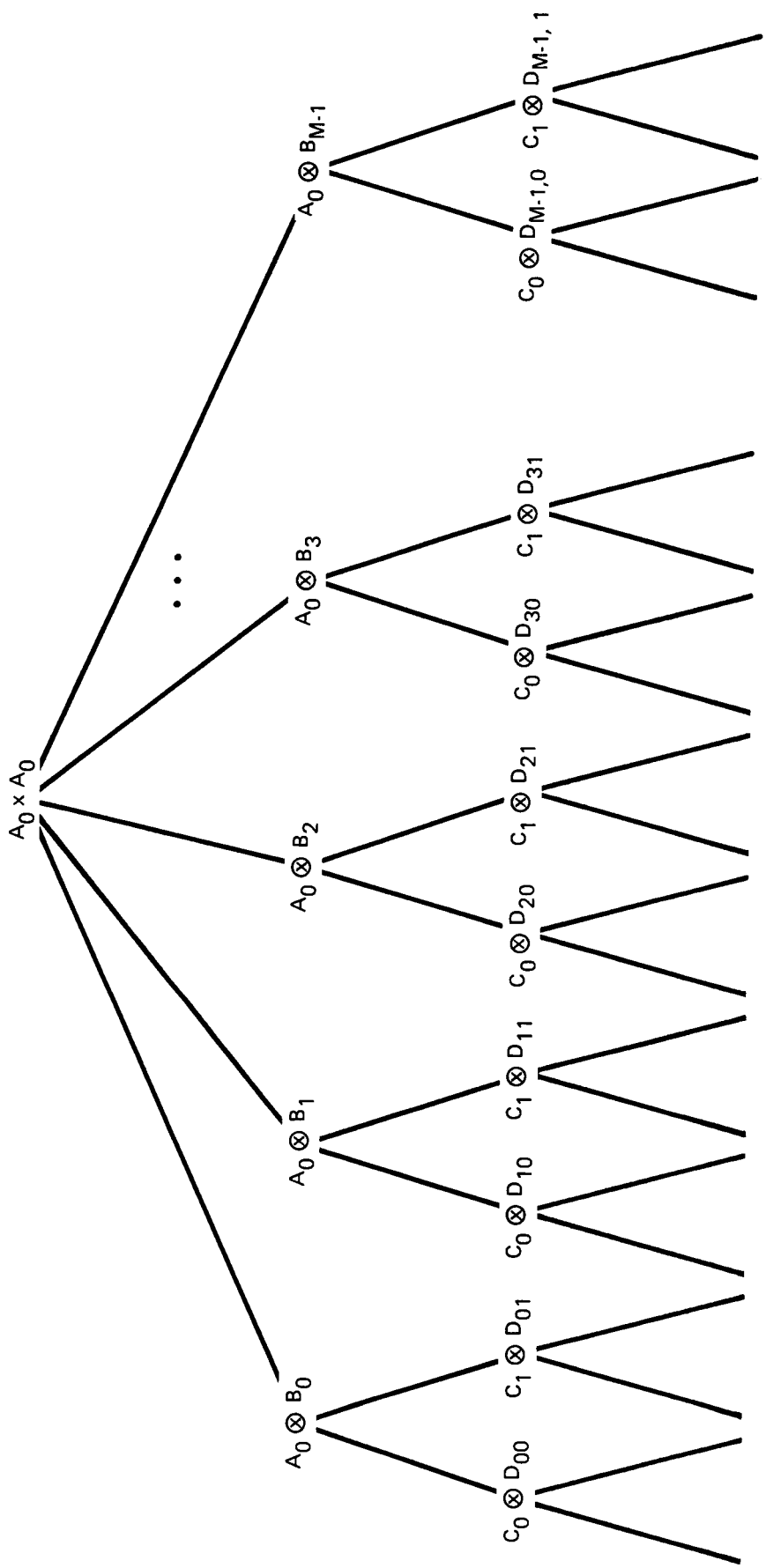

Figure 8. Set Partitioning Method for Multiple (k = 2) Trellis Codes on the Fading Channel

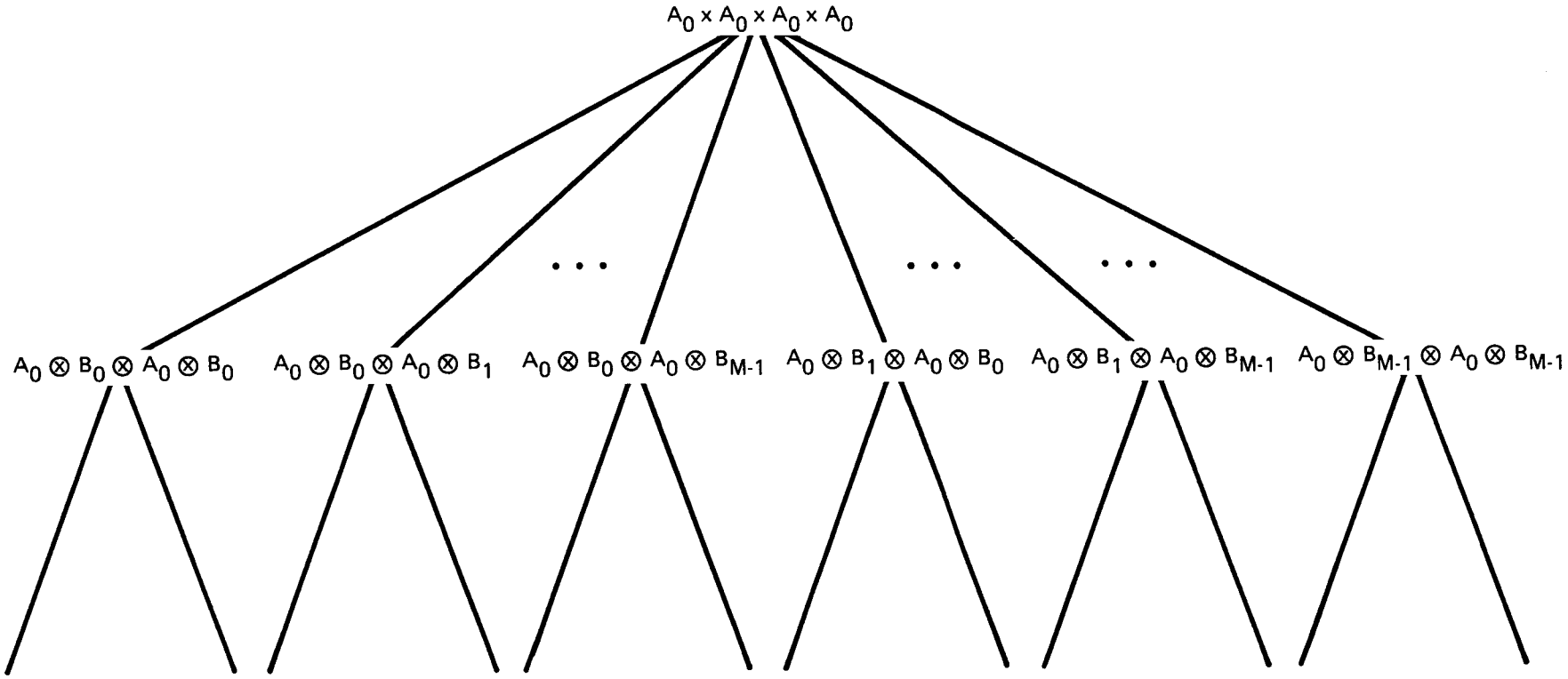

Figure 9. Set Partitioning Method for Multiple Trellis Codes on the Fading Channel

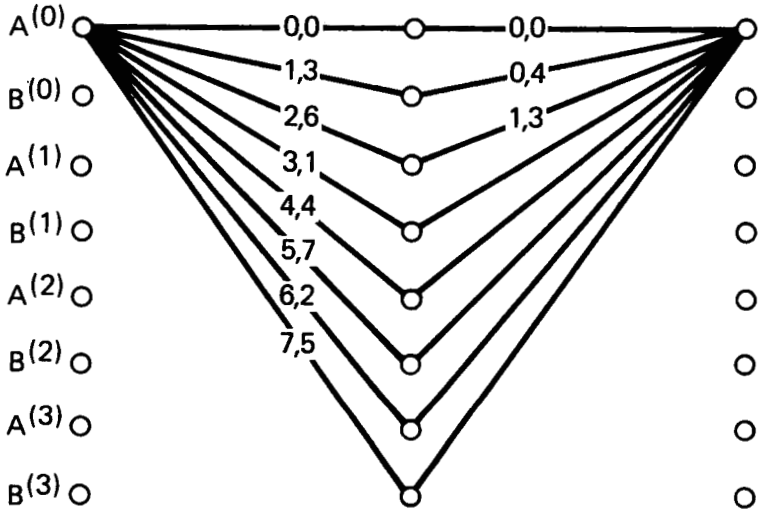

Figure 10. Trellis Diagram for Rate 3/6 Trellis Coded 8PSK

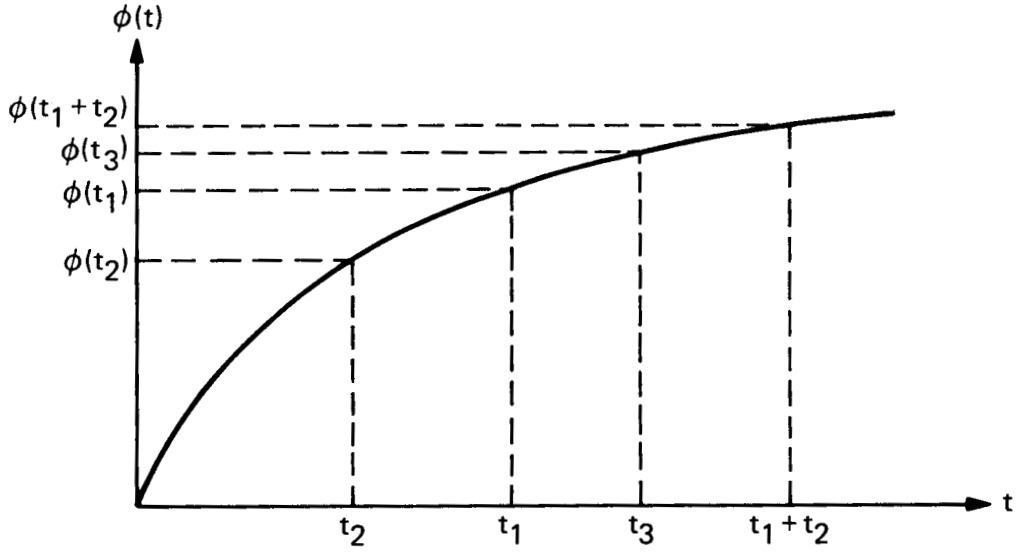

Figure A-1. An Example of a Function that Satisfies the Conditions for a Metric